2019-01-01

Comparative Study Of Analytical Models Of The Gruneisen Parameter Of Metals As Function Of Pressure

Celia Garcia Amparan
University of Texas at El Paso

COMPARATIVE STUDY OF ANALYTICAL MODELS

OF THE GRUNEISEN PARAMETER OF METALS

AS FUNCTION OF PRESSURE

CELIA GARCIA AMPARAN

Master's Program in Metallurgical and Materials Engineering

APPROVED:

Ramon Ravelo, Ph.D., Chair

Steve Stafford, Ph.D.

Russell Chianelli, Ph.D.

Jose Bañuelos, Ph.D.

Stephen Crites, Ph.D.
Dean of the Graduate School

Dedicado a Mi Mamá

¡Te Quiero!

In this work, when it shall be found that much is omitted, let it not be forgotten that much likewise is performed...

Samuel Johnson, A.M.

From Preface to Dictionary of the English Language,
Vol. 1, page 5, 1755, London, Printed by Strahan.

COMPARATIVE STUDY OF ANALYTICAL MODELS OF THE GRUNEISEN PARAMETER OF METALS AS FUNCTION OF PRESSURE

by

CELIA GARCIA AMPARAN, B.S.

THESIS

Presented to the Faculty of the Graduate School of

The University of Texas at El Paso

in Partial Fulfillment

of the Requirements

for the Degree of

MASTER OF SCIENCE

Department of Metallurgical and Materials Engineering

THE UNIVERSITY OF TEXAS AT EL PASO

August 2019

Acknowledgements

This stage of my life is made all the more possible thanks to my advisor Dr. Ramon Ravelo of the Physics Department at The University of Texas at El Paso. His amazing explanations always leave me in awe of how dedicated he is to our field. Dr. Ravelo is one of the few people I have come to trust and will always admire. Thank you for your patience and constant support.

In this work and in my career I am particularly lucky to count with my partners support. Brandon always shows me limitless understanding, even when I am my most frustrating and un-agreeable self. Much affection and gratitude to my parents, Celia and Antonio, for their trust in my path. Our hard work will pay off.

Deep gratitude to Dr. Steve Stafford for introducing me to the field of material engineering in my undergraduate years and for agreeing to being a part of this process. Finally, to the other members of my committee, Dr. Russell Chianelli of The Materials Research and Technology Institute and Dr. Jose Bañuelos of the Physics Department, both at The University of Texas at El Paso. This could not be possible without them. Thank you for being a part of this process.

Abstract

Commonly used Gruneisen parameter (γ) models only hold accurate in limited regimes making them inapplicable for use over wide temperature-pressure conditions. The accuracy of these analytical models of γ and of the thermal expansion of solids are of particular interest as these are considered proxies for quantifying anharmonicity, which may be a significant contribution to the thermal pressure at high temperatures. This work reviews various definitions of γ and their relations to the equations of state and applies them to two simple metals: Tantalum (Ta) and Copper (Cu), for which a high body of experimental data exists. Classical Molecular Dynamics simulations are employed in both constant temperature and constant pressure formalisms to obtain pressure and volume data over wide temperature-pressure conditions. We discuss the dependence of γ with pressure focusing on Ta and Cu as examples and compare our results with predictions from commonly used analytical models of γ and experimental data.

Table of Contents

List of Tables

List of Figures

Chapter 1

Introduction

Material models are used to predict and understand material behavior at the micro and macro scales. These models serve the acceleration of material research by facilitating the prediction of behavior under conditions otherwise difficult to observe. Wide-regime models are of immediate interest in areas such as planetary physics, thermonuclear fusion, geophysics, and other multidisciplinary applications [1].

There are several means of developing material models. Most however boil down to the theoretical, also referred to as mechanical, and the first principle approaches. Mechanical models approach macro scale behavior with the help of Equations of State (EoS) developed off available experimental data. On the other hand, the first principle approach is based on the atomic interactions within the material.

These approaches are not without limitation. Mechanical models depend on, and demand, a large number of experimental data sets. This becomes problematic due to the age of available data, and because of human nature as Edward L. Brady brilliantly explains:

> *The man who wants to use existing data, rather than make new measurements himself, faces a long and costly task if he wants to assure himself that he has found all the relevant results. More often than not, a search for data stops after one or two results are found– or after the searcher decides he has spent enough time looking.*
>
> From Thermophysical Properties of Matter, Vol. 12, 1975, New York, Printed by Plenum Publishing [2].

On the other hand, for first principle calculations the computational cost increases with the size of the problem. This makes first principle calculations extremely dependent on

efficient theoretical and computational techniques.

The literary review shows, on the surface, models capable of effectively duplicating well understood material properties. Further observation reveals that efforts to predict more intricate properties are hampered by the complexity associated with their calculation. Thermal conductivity and the Gruneisen parameter (γ) are good examples of this type of computationally complex properties [3] [4]. The Gruneisen parameter and its many analytical models are of particular interest in this work. Table 1.1 shows the difficulty in determining which γ definition is most reliable, even among particular elements or categories like transition metals.

It is important that contemporary researchers not assume any models accuracy. How the models in this work fail or succeed will give valuable insight as to which approach is most worthy of attention and future development. The purpose of this work is then to quantitatively investigate the differences and similarities between several models to for γ under a wide temperature-pressure regime. Two simple materials, Tantalum (Ta) and Copper (Cu), were decided upon to illustrate each models performance.

Computational techniques, mainly Classical Molecular dynamics (MD) were used for data collection. MD makes use of embedded atom (EAM) potentials to approximate each materials energy and behavior. Most potentials are classical and not from first principle calculations. That is to say, these potentials are build using the available experimental data as adjusting parameters. The EAM potentials for Ta and Cu in this work were selected thanks to their previously documented and satisfactory performance [5] [6].

Table 1.1: The Gruneisen parameter, γ, of various materials. The values vary depending on the definition use. Note: γ = Thermodynamic definition; γ_S = Slater definition; γ_{DM} = Dugdale-MacDonald definition; γ_{VZ} = Vashchenko-Zubarev definition [11] [12] [13] [14] [15].

Material	γ	γ_S	γ_{DM}	γ_{VZ}
Al	2.14	1.97	1.64	1.30
$Al_2\ O_3$	1.13	1.92	1.59	1.25
Cu	1.97	1.30	2.60	1.92
Fe	1.65	2.65	2.31	1.98
$MgAl_2O_4$	1.40	2.10	1.84	1.51
MgO	1.54	1.12	0.78	0.45
Mg_2SiO_4	2.18	2.39	2.05	1.72
Mo	1.60	2.10	1.75	1.42
Ta	1.62	1.67	1.35	1.01
W	1.71	2.0	1.67	1.33

1.1 Harmonicity, Anharmonicity and Quasi-Harmonicity

Many material properties can be interpreted in terms of the harmonic approximation. These include lattice specific heat and thermal diffuse scattering. Atoms in a material lattice can be though of as oscillators about their equilibrium positions, separated by equilibrium distance r_{eq}. This system can be represented by a parabolic or symmetrical interatomic pair potential when the restoring force $F_{res} = k(r - r_{eq})$ is proportional to the elongation $r - r_{eq}$. The harmonic approximation performs well at low energy but becomes less accurate as the energy increases. There is also no presence of thermal expansion or phonon interaction.

Deviation from the harmonic approximation is most relevant at high temperatures. In an anharmonic system r_{eq} is determined by the balance of long-rage attractive and short-range repellent forces, steeper towards smaller interatomic distances. The interatomic pair potential is then asymmetrical. As the interatomic spacing decreases the restoring force increases rapidly and the isothermal bulk modulus B_T increases with pressure. The harmonic and anharmonic curves can only be assimilated near their minima, the quasi-harmonic region of the anharmonic pair potential. This is possible thanks to the low vibration of the atoms at lower temperatures.

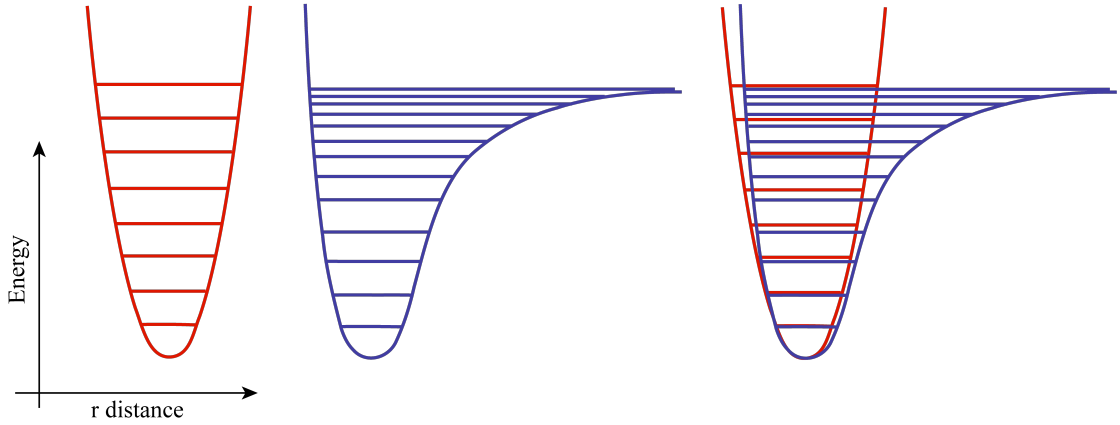

Figure 1.1: Harmonic (red) and anharmonic (blue) interatomic pair potential curves. The curves show the energy of a system as a function of the separation distance. Note how the two curves can be assimilated near their minima; this is the quasi-harmonic region.

1.1.1 Thermal Expansion

The anharmonicity of the pair potential curve at high temperatures can be seem as the cause of thermal expansion. This is thanks to the materials phonon gas acquiring a finite temperature-dependent pressure. Linear thermal expansion is referred to as α in this work. At low temperatures the system is more harmonic and α approaches zero. The exact functional dependence with which it approaches this limit depends on the particular material. Note that α is not automatically zero for harmonic materials (as cases where $B' = 1$ and γ is negative implies α to also be negative [16]). Nor is B_T independent of pressure.

The linear thermal expansion coefficient at constant volume is obtained with the use an approximation for isotropic solids, $\alpha = \frac{\beta}{3}$.

$$\beta = \frac{1}{V}(\frac{\partial V}{\partial T})_P = -\frac{1}{V}(\frac{\partial V}{\partial P})_T(\frac{\partial P}{\partial T})_V = \frac{1}{B_T}(\frac{\partial P}{\partial T})_V \tag{1.1}$$

$$\alpha = \frac{1}{3V}(\frac{\partial V}{\partial T})_P = \frac{1}{3B_T}(\frac{\partial P}{\partial T})_V \tag{1.2}$$

Where β is the volumetric thermal expansivity, V is the volume, T is the temperature, P is the pressure and B_T is the bulk modulus. Equation (1.2) relates to the Gruneisen parameter as:

$$\alpha = \frac{1}{3V}(\frac{\partial V}{\partial T})_P = \frac{1}{3B_T}(\frac{\partial P}{\partial T})_V = \frac{\gamma C_V}{3B_T V} \tag{1.3}$$

Recall that for a harmonic system α approaches zero as C_V approach zero with decreasing temperature. Observing α in this way means that at zero pressure γ becomes a non zero constant. This α-γ relation can thus serve as a proxy for quantifying anharmonicity.

Experimentalist Approach

Experimental data for α in Ta and Cu can be seen in Figures 1.2 and 1.3, respectively. The figures were generated with the use of critically evaluated and recommended data from Touloukian *et. al.* Vol. 12 (1975) [2]. It should be noted that such data is in the minority of what is contained in the volume for each material.

Linear thermal expansion is calculated from physical specimens, with the first given temperature as the reference temperature.

$$\alpha = \frac{\Delta L/L_0}{\Delta T} \tag{1.4}$$

Where $\Delta L/L_0$ is the fractional change in length, and ΔT is the change in temperature. Specialty equipment is used (i.e., telemocroscopes, push-rob dilatometers, and interferometers) to calculate $\Delta L/L_0$.

The twin-telemicrocope method measures expansion of larger specimens at high temperatures. This setup is that of two telemicroscopes with filar micrometer eyepieces mounted on low expansion support robs to face furnace windows. Each telemicroscope is then calibrated so that the planes of focus coincide.

Push-rob dilatometers work by placing the specimen inside a chamber in a tubular furnace. A push-rob is placed against the specimen. The changes in length and corresponding temperature are recorded by a linear variable displacement transducer and a thermocouple. The dilatormeter later applies a calibration correction curve to account for the expansion of the push-rob and the chamber.

Iterferometers measure the change in length expressed by a number of wavelengths.

$$\Delta L = \frac{n\lambda}{2} \tag{1.5}$$

Where n is the number of fringe shifts, and λ is the wavelength of a laser light. The denomicator is dictated by the mirrors in the setup i.e., when the mirrors move a distance x the path length changes by $2x$. This results in the linear coefficient of thermal expansion

definition:

$$\alpha = \frac{n\lambda}{2L_0\Delta T} \tag{1.6}$$

Note that experimental data still requires evaluation, as too often there are discrepancies in the results by various experimentalists.

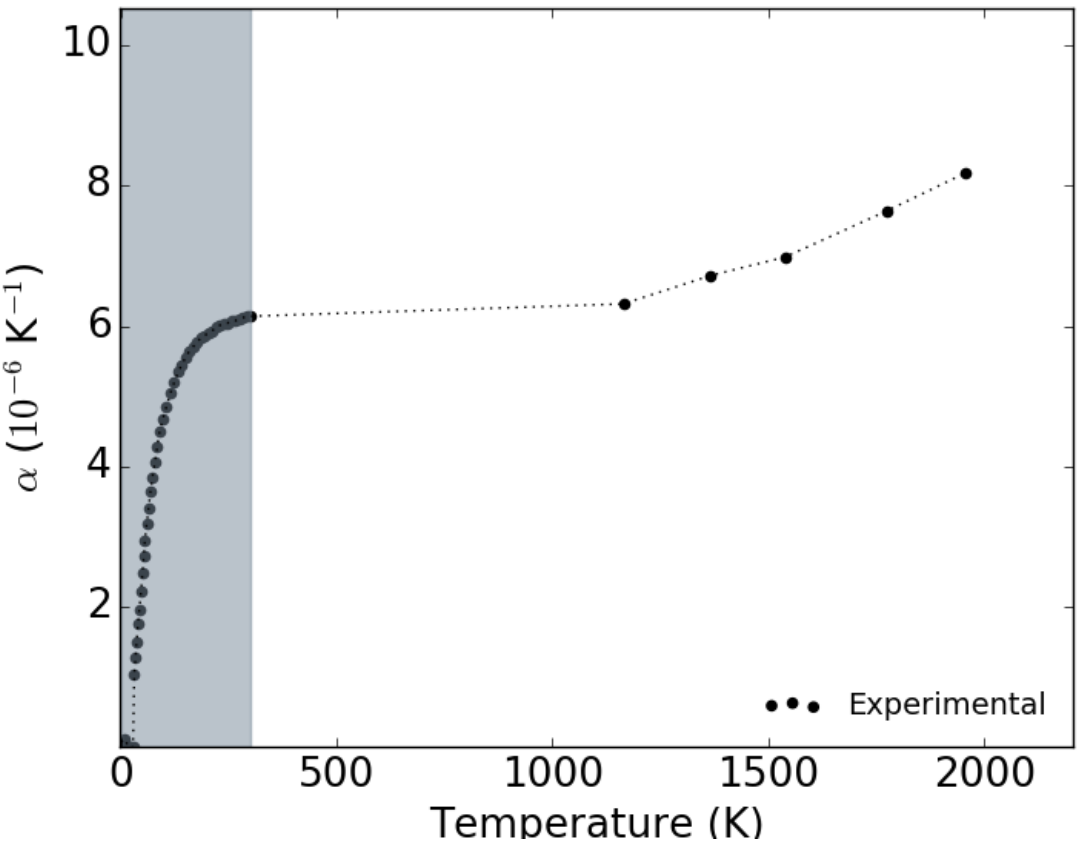

Figure 1.2: Thermal linear expansion coefficient α of Tantalum. The low temperature (more harmonic) region is shown in gray. A wider range of curves can be found in Touloukian *et. al*. 1975 [2]. Shown here are only critically evaluated and recommended values.

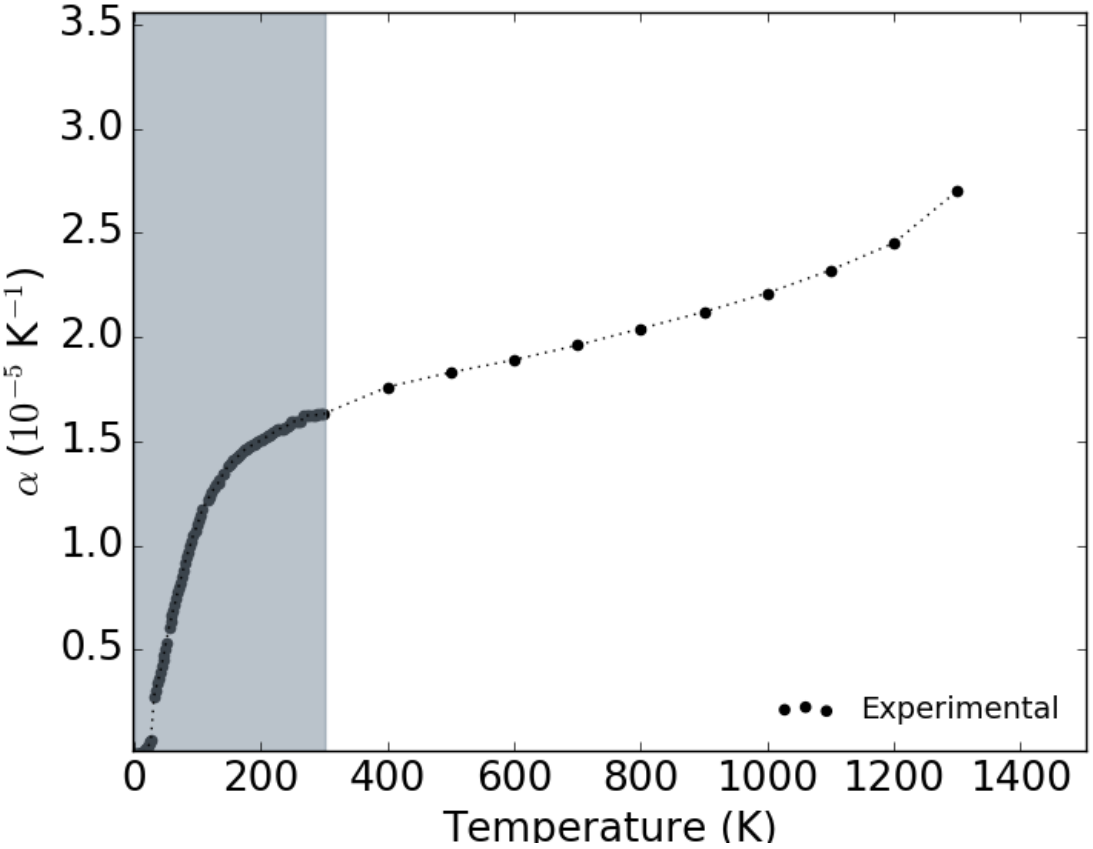

Figure 1.3: Thermal linear expansion coefficient α of Copper. The low temperature (more harmonic) region is shown in gray. A wider more detailed range of curves can be found in Touloukian *et. al.* 1975 [2]. Shown here are only critically evaluated and recommended values.

1.2 The Gruneisen Parameter

The Gruneisen parameter is, in the simplest of terms, a dimensionless value which arises from a combination of familiar material properties. As mentioned in Section 1.1.1 it can be used as a measure of the anharmonicity that arises from asymmetric atomic vibrations. Work as recent as S. A. Miller *et. al.* 2017 [17] has made use of this fact to improve the accuracy of existing models [18]. The Gruneisen parameter was however treated as a constant by Miller *et. al.* by using the average γ value of materials with a particular coordination number. With experimentally measured γ values ranging from 0.5 to 2 for a coordination number range of 3 to 6, why wouldn't γ be calculated explicitly? Aside from lowering computational costs.

There is a long history of definitions used for the calculation of the Gruneisen parameter; some of which are known to yield conflicting results [19] [20]. The conflicts mostly arise from each of their derivations, which cary their own set of assumptions [21]. Table 1.2 provides the names and notation for various Gruneisen parameter definitions.

The true definition of the Gruneisen Parameter at constant volume can be written as:

$$\gamma = V(\frac{\partial P}{\partial E})_V \tag{1.7}$$

Where E is internal energy, V is volume, and P is pressure. Note that γ is expressed as the change in pressure with respect to the energy density. Equation (1.7) provides a pressure-temperature relation thanks to the proportional nature of energy and temperature.

Table 1.2: Various definitions for calculating the Gruneisen parameter. The name of each model is provided along with the models notation. References are provided. Note: Approximations are shown with subscripts.

Name of Model	Notation	Ref.
Debye-Brillouin Gruneisen parameter	γ_B	Quareni and Mulargia (1988)
Dugdale-MacDonald Gruneisen parameter	γ_{DM}	Dugdale and MacDonald (1953)
Mode Gruneisen parameter	γ_i	Gruneisen (1912)
Thermodynamic Gruneisen parameter	γ	e.g., Barron (1957)
Vashchenko-Zubarev Gruneisen parameter	γ_{VZ}	Vashchenko and Zubarev (1963)
Slater Gruneisen parameter	γ_S	Slater (1939)

Chapter 2

Gruneisen Parameter Models

The Gruneisen parameter as defined by equation (1.7) has been seen as inconvenient. This view is largely due to its need for thermal energy data at varying pressure, which is difficult to obtain experimentally (aside from computational techniques) [22]. To remedy this, approximate definitions of γ were developed by multiple experimentalist of the time based on a variety of assumptions. The use of these models has for a long time been a matter of personal choice. The most commonly used models relate γ at zero pressure to the first derivative of the bulk modulus. For calculations at varying, non-zero, pressures $\gamma(P)$ became a function of an equation of state.

2.1 Equations of State

Equations of state (EoS) are used in order to express the thermodynamic state of a material. These EoS serve as functional relationships between properties such as pressure, temperature, and volume. A well known example of this is the ideal gas law:

$$PV = nRT \tag{2.1}$$

Where P is gas pressure, V is the volume taken up by the gas, n is the number of moles of gas, R is the universal gas constant, and T is temperature.

A focus of this work is to look at the applicability of EoS for the calculation of thermodynamic properties. For example, a simple isothermal EoS is given by the definition of the bulk modulus.

$$B_T = -\frac{\partial P}{\partial lnV} = \frac{\partial P}{\partial ln\rho} \tag{2.2}$$

Where P is pressure, V is volume and ρ is density. In the case of linear elasticity, with constant bulk modulus, the EoS is found by integrating equation (2.2):

$$V = V_0 \; exp[-\frac{P}{B_0}] \tag{2.3}$$

Note however that this EoS fails at high pressures as it does not take into account the increase of B_T with pressure, i.e., compression becoming more difficult. Other EoS are given by the definition of the volumetric strain ε.

$$\varepsilon = -\frac{\partial V}{V_0} = 1 + \beta(T - T_0) \tag{2.4}$$

$$V = V_0 \; [1 + \beta(T - T_0)] \tag{2.5}$$

$$V = V_0 \; exp[\beta(T - T_0)] \tag{2.6}$$

Where V is volume, β is the volumetric thermal expansion coefficient, and T is temperature. Equations (2.5) and (2.6) correspond to low temperature and high temperature ranges, respectively.

Above the materials Debye temperature T_D, it is appropriate to use the general form of the Mie-Gruneisen EoS:

$$P(V,T) = P(V,0) + P_{Th}(V,T) \tag{2.7}$$

and,

$$P_{Th}(V,T) = P(V,T) - P(V,0) = \frac{\gamma}{V} E_{Th} \tag{2.8}$$

Where $P(V,T)$ is the pressure at each volume V and corresponding temperature T, $P(V,0)$ is the cold (0K) pressure, P_{Th} is the thermal pressure, E_{Th} is the thermal energy, and γ is the Gruneisen parameter. Using the thermal energy relation to the specific heat capacity and temperature, $E_{Th} = C_V T$, equation (2.8) becomes:

$$P(V,T) - P(V,0) = \frac{\gamma}{V} C_V T \tag{2.9}$$

and it is then possible to isolate γ from the Mie-Gruneisen EoS as,

$$\gamma_{EoS} = \frac{[P(V,T) - P(V,0)]V}{C_V T} \tag{2.10}$$

2.2 Mechanical Gruneisen Models

A variety of experimental hindrances, approachable now with the use of computational techniques and ab initio calculations, encouraged at the time the development of other approximate models of γ. These were developed to avoid complex experimental conditions. Three of these models, most commonly found in the literature, involve the bulks modulus and pressure.

The Slater model for γ at zero pressure is obtained as:

$$\gamma_S = \frac{1}{2} B_0' - \frac{1}{6} \tag{2.11}$$

For a harmonic potential $\gamma_{Sl} = 1/3$. One of the main known limitations of the Slater model is in its view of acoustic velocities as independent of pressure; properties which are in reality strongly connected [24].

The following mechanical models can be seen as improvements to γ_S. The model by Dugdale and MacDonald is written as:

$$\gamma_{DM} = \frac{\frac{1}{2} B' - \frac{1}{2} - \frac{1}{9} \frac{P}{B_T}}{1 - \frac{2}{3} \frac{P}{B_T}} \tag{2.12}$$

And at zero pressure as:

$$\gamma_{DM} = \frac{1}{2}B_0' - \frac{1}{2} \tag{2.13}$$

This equation proposed a correction to γ_S by accounting for the effect of finite strain under pressure. It also used one-dimensional oscillations with interatomic nteractions.

The free volume model by Vaschenko and Zubarev γ_{VZ} is written as:

$$\gamma_{VZ} = \frac{-\frac{5}{6} + \frac{1}{2}B' + \frac{2}{9}(\frac{P}{B_T})}{1 - \frac{4}{3}(\frac{P}{B_T})} \tag{2.14}$$

And at zero pressure as:

$$\gamma_{VZ} = \frac{1}{2}B_0' - \frac{5}{6} \tag{2.15}$$

These definitions can also be expressed together in the generic equation (5.5):

$$\gamma(V) = \frac{[\frac{B'}{2} - \frac{1}{6} - \frac{t}{3}](1 - \frac{P}{3B_0})}{[1 - \frac{2t}{3}\frac{P}{B_0}]} \begin{cases} t = 0 & (\gamma_S) \\ t = 1 & (\gamma_{DM}) \\ t = 2 & (\gamma_{VZ}) \end{cases} \tag{2.16}$$

Where P is the pressure from the cold curve (T=0 equation of state). Again the pressure dependence comes from the relations B_T and B', which are linked to the materials bond asymmetry.

2.3 Vibrational Gruneisen Model

Thermal effects can be quantized in terms of lattice vibration. This is done by retaining the harmonic expression in Helmholtz free energy while introducing a volume dependence on the phonon vibration frequencies. This gives the following EoS:

$$F_{QHA}(V,T) = E_0(V) + F_{vib}(V,T) + F_e(V,T) \tag{2.17}$$

$$F_{vib}(V,T) = \frac{1}{N_{\overline{k}}} K_B T \sum_{\overline{k},n} ln[2sinh(-\frac{\hbar\omega_{n,\overline{k}}(V)}{2K_B T})] \tag{2.18}$$

Where $E_0(V)$ is the zero-temperature internal energy, F_{vib} is the vibrational free energy lattice ions, and F_e is the free energy due to the thermal excitation of electrons. The quasi-harmonic approximation (QHA) takes into account thermal effects via volumetric changes caused by thermal expansion. It should be noted however that QHA does not account for all the anharmonic effects that arise from changes in temperature [26] [27] [28].

Other thermodynamic properties are then derivable from the corresponding relation to F_{QHA}. The bulk modulus B_T, is obtained by taking an isothermal second derivative of equation (2.17) with respect to the volume V:

$$B_T = V(T)(\frac{\partial^2 F_{QHA}}{\partial V^2})_T \tag{2.19}$$

Taking the first derivative of equation (2.17) with respect to V yields the equation for thermal pressure as:

$$P = -(\frac{\partial F_{QHA}}{\partial V})_T \tag{2.20}$$

The low temperature ($T < T_D$) vibrational Gruneisen parameter γ_{Vib}, can be seen as another approximation to γ. This approximation assumes quasi-harmonic material lattice dynamics, and solely volume dependent normal-mode frequencies $\omega_{n,\overline{k}}(V)$.

$$\gamma_{Vib}(V,T) = \frac{\sum_{n,\overline{k}} \gamma_{n,\overline{k}}(V) c_{n,\overline{k}}(V,T)}{\sum_{n,\overline{k}} c_{n,\overline{k}}(V,T)} \tag{2.21}$$

$$\gamma_{n,\overline{k}}(V) = -\frac{\partial[ln\omega_{n,\overline{k}}(V)]}{\partial(lnV)} \tag{2.22}$$

$$c_{n,\overline{k}}(V,T) = [\frac{\hbar\omega_{n,\overline{k}}(V)}{K_B T}]^2 \frac{e^{\hbar\omega_{n,\overline{k}}(V)/K_B T}}{[e^{\hbar\omega_{n,\overline{k}}(V)/K_B T} - 1]^2} \tag{2.23}$$

Where $\gamma_{n,\overline{k}}(V)$ is the normal-mode Gruneisen parameter, $c_{n,\overline{k}}(V,T)$ is the normal-mode $(\overline{k},n)$ contribution to the specific heat $c_{n,\overline{k}}(V,T)$, $\overline{k}$ is the wave vector and n is the branch index.

At temperatures higher than $\hbar\omega_{max}(V)/K_BT$ the heat capacity can be found as:

$$C_V = 3NK_B \tag{2.24}$$

Where N is the number of atoms per unit cell. The vibrational Gruneisen parameter (classical limit $T > T_D$) is then the average value of the normal-mode Gruneisen parameters, $\gamma_{Vib}(V) = \langle\gamma_{n,\overline{k}}\rangle$.

Chapter 3

Molecular Dynamics

3.1 Classical Molecular Dynamics and Force

Molecular Dynamics is one of the main computational techniques used to predict the behavior and time evolution of a system of interacting atoms in a crystalline material system [25]. The basics behind MD simulations consist of calculating numerical solutions for the classical equations of motion governing each of the atoms. Atomic positions and velocities, for example, are found by calculating F=ma for each atom at each time step δt.

The equations of motion are integrated over time based on the EAM potential dictating the atomic behavior. The initial position, velocity, etc., at time t is used to calculate the same properties at a later time, t+δt. This is done with enough accuracy by using a suitable algorithm for integration of the equations of motion (Verlet Algorithm). Note that δt should be smaller than the process being observed, e.g., femtoseconds (10^{-15} or one millionth of one billionth of a second) depending on the atomic vibration frequency. The atomic position of atom i at time t is represented by $r(t)$, defining the position at time t+δt and t-δt as:

$$\overline{r}(t+\delta t) = \overline{r}(t) + \delta t\overline{v}(t) + \frac{1}{2}\delta t^2\overline{a}(t) + \frac{1}{3!}\delta t^3\overline{b}(t) + O(\delta t^4)... \tag{3.1}$$

$$\overline{r}(t-\delta t) = \overline{r}(t) - \delta t\overline{v}(t) + \frac{1}{2}\delta t^2\overline{a}(t) - \frac{1}{3!}\delta t^3\overline{b}(t) + O(\delta t^4)... \tag{3.2}$$

The two Taylor expansions (3.1) and (3.2) can then be used to obtain velocities and positions at previous and subsequent points in time. Note that while velocities display

only second order numerical accuracy, the positions are already highly accurate (4th order accuracy).

$$\overline{v}(t+\delta t) = 2\overline{r}(t) - \overline{r}(t-dt) + \delta t^2 \overline{a}(t) + ... \tag{3.3}$$

The Verlet algorithm is time reversible in nature, $\overline{v}(t+\delta t)$ and $\overline{v}(t-\delta t)$, ensuring conservation of momentum.

The often used "leap-frog" method is obtained by rearranging the basic form of the Verlet algorithm. The positions are calculated at integer values of δt, and the velocities at half-integer values.

$$\overline{r}(t+\delta t) = \overline{r}(t) + \overline{v}(t+\frac{1}{2}\delta t)\delta t \tag{3.4}$$

$$\overline{v}(t+\frac{1}{2}\delta t) = \overline{v}(t-\frac{1}{2}\delta t) + \overline{a}(t)\delta t \tag{3.5}$$

The acceleration of each atom is calculated from the force, which is evaluated from the interaction between the atom and its neighbors within the simulation box. Periodic boundary conditions limit the size of the simulation box in order to alleviate cost while retaining the essence of longterm (infinite) simulations. This cutoff distance depends on the particular EAM potential in use.

In principle these calculations are performed quickly. The numerical analysis however can become costly depending on the time step length and the number of atoms in the simulation. To further reduce simulation cost ensemble averages are used over statistically complex time averages. This can be done thanks to the ergodicity of the system, where the time averages are the same as the averages over the probability space [29].

3.1.1 Calculating Macroscopic Properties

Ensemble averages provide a functional path to calculate macroscopic thermal properties (e.g., volume, pressure or energy) from the microscopic atomic interactions within the

system [30]. For stationary ensembles the average value of the energy will be independent of time. That is to say, the system will be in equilibrium. A system with constant statistical temperature T and constant number of atoms N restricted to a fixed volume V is termed NVT or canonical. A system with constant statistical temperature T and constant number of atoms N restricted to a fixed pressure P is termed NPT or isothermal-isobaric.

Canonical Ensemble

NVT ensemble are carried out by modulating the temperature of the system through a The Nosè-Hoover thermostat [31]. This thermostat interacts with the atoms to obtain the desired average temperature. It also couples the temperature of the system to a heat bath, and introduces an extra degree of freedom to represent the thermal reservoir. The atoms exchange energy dynamically with the reservoir. The Nosè-Hoover equations of motion for NVT ensembles are defined as:

$$\dot{v}_\alpha = \frac{F_\alpha}{m} - v_p \zeta v_\alpha \tag{3.6}$$

$$\dot{\zeta} = v_T(\frac{T}{T_0} - 1) \tag{3.7}$$

Where v_p and v_T are coupling-rate parameter frequencies, and ζ is the frictional coefficient. Adjusting ζ allows the system to reach equilibrium for statistical temperature T_0, while the value of T fluctuates with thermal energy.

Isothermal-Isobaric Ensemble

NPT ensemble are carried out much like NVT ensembles and are defined as:

$$\dot{r}_\alpha = v_\alpha + v_P \eta_\alpha r_\alpha \tag{3.8}$$

$$\dot{v}_\alpha = \frac{F_\alpha}{m} - (v_p \eta_\alpha + v_T \zeta) v_\alpha \tag{3.9}$$

$$\dot{\zeta} = v_T(\frac{T}{T_0} - 1) \tag{3.10}$$

where η_α is a strain-rate variable.

3.2 Embedded Atom Potentials

EAM potentials are used to approximate the computational potential energy of a system of atoms. They are based on density functional theory where the total energy of the system is considered as a function of atomic positions. Equation (3.11) present the total energy as:

$$E_{tot} = \sum_i F(\overline{\rho_i}) + \frac{1}{2}\sum_{i,j} \phi_{ij}(R_{ij}) \tag{3.11}$$

Where $F(\overline{\rho_i})$ is the embedding energy and ϕ_{ij} is a pair potential between atoms i and j, separated by radial distance R_{ij}. It follows that the energy per atom, E_i, is:

$$E_i = F(\overline{\rho_i}) + \frac{1}{2}\sum_j \phi(R_{ij}) \tag{3.12}$$

Where the embedding density ρ_i is:

$$\rho_i = \sum_{j \neq i} f(R_{ij}) \tag{3.13}$$

And f is a spherically symmetric function. The proper potential is vital for accurate MD simulations as this force equals the gradient of the potential, $F = - \bigtriangledown \phi$.

3.2.1 Potentials in this Work

Potentials are adjusted to, and should agree with, previous experimental data. Note that all-accurate wide regime potentials are difficult to create. It is worth highlighting the impact of the potentials' construction. Two EAM potentials for the same material, constructed using various approaches or calibrated to different experimental data sets, can yield comparable or unequal results. Therefore, it is essential to review available EAM potentials in order to decide which are best suited for the demands of a particular simulation.

Lattice Properties

Suitable EAM potentials were necessary to perform computational simulations for Tantalum and Copper. Tables 3.2 and 3.4 show how the potentials in this work effectively reproduce the values of relevant properties such as lattice constant a_0; cohesive energy E; bulk modulus B_0; and elastic constants C_{11}, C_{12}, C_{44}. For Ta the potential Ta 2, developed by R. Ravelo *et. al.* 2013 [5] was used. Potential EAM 1 was used for Cu, developed by Y. Mishins *et. al.* 2001 [6]. As additional confirmation, the thermal expansion coefficient of Cu was also calculated from MD and compared to experimental data at zero pressure. The EAM 1 potential demonstrates agreement with experimental data and can be seen in Figure 6.2.

Equations of State

The cold curves of the materials were calculated and can be seen in Figures 3.2a and 3.3a. Figure 3.2b demonstrates how the Tantalum potential in this work is in agreement with experimental pressure data [7] [8] under strong compression. Likewise, Figure 3.3b demonstrates that the Copper potential in this work is in agreement with experimental pressure data [9] [10] under strong compression.

Table 3.1: Some optimizing parameters of the embedded atom potential Ta 2. A full outline of parameters can be found in Ravelo *et. al.* 2013, Table 1 [5].

Parameter	Value
E(eV)	8.1
$a_0(\dot{A})$	3.304
$\alpha(\dot{A}^{-1})$	4.950
$r_s(\dot{A})$	2.8683

Table 3.2: Properties of Tantalum calculated with embedded atom potential Ta 2 compared with known experimental data. A full outline of properties can be found in Ravelo *et. al.* 2013, Table 2 [5].

	Experiment	Ta2
a_0 $(\dot{A})$	3.304	3.304
E (eV/atom)	-8.100	-8.100
C_{11}(GPa)	264	267
C_{12}(GPa)	160	160
C_{44}(GPa)	82	86
B_0'	3.4	3.9

Table 3.3: Some optimized parameters of embedded atom potential EAM 1. A full outline of the optimized parameters can be found in Mishin *et. al.* 2001, Table 1 [6].

Parameter	Value
E_1 (eV)	$2.01458 * 10^2$
E_2 (eV)	$6.59288 * 10^{-3}$
$a_0(\dot{A})$	3.80362
$\alpha_1(\dot{A}^{-1})$	2.97758
$\alpha_2(\dot{A}^{-1})$	1.54927
$r_s^{(1)}(\dot{A})$	2.24
$r_s^{(2)}(\dot{A})$	1.80
$r_s^{(3)}(\dot{A})$	1.20

Table 3.4: Properties of Copper calculated with embedded atom potential EAM 1 compared with known experimental data. A full outline of properties can be found in Mishin *et. al.* 2001, Table 3 [6].

	Experiment	EAM1
a_0 $(\dot{A})$	3.615	3.615
E (eV/atom)	-3.54	-3.54
$C_{11}(10^{11}\text{Pa})$	1.700	1.699
$C_{12}(10^{11}\text{Pa})$	1.225	1.226
$C_{44}(10^{11}\text{Pa})$	0.758	0.762
$B(10^{11}\text{Pa})$	1.383	1.383

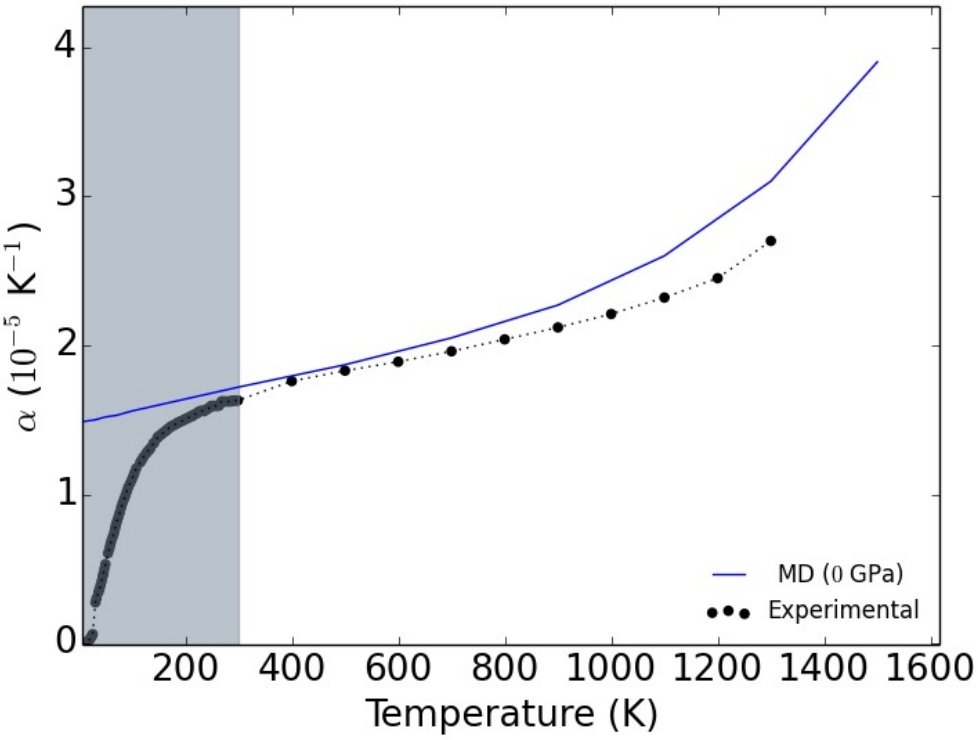

Figure 3.1: Comparison between thermal linear expansion coefficients of Copper calculated with the use of potential EAM 1 [6], shown in blue. The dashed line shows experimental data included for comparison [2]. Note the low temperature region is shown in gray (0 to 246 K).

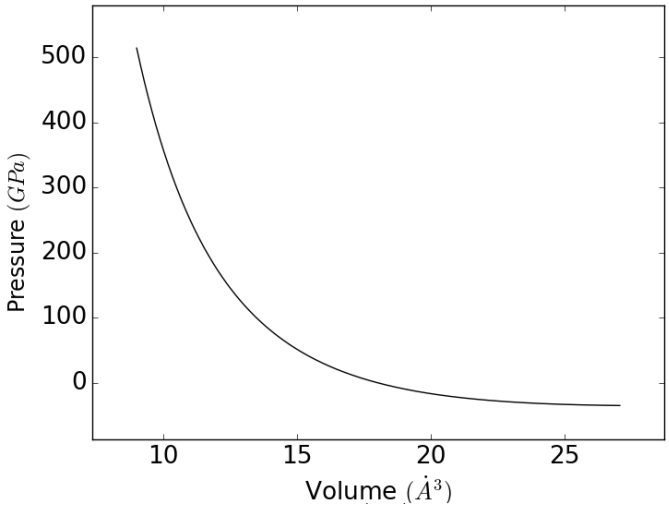

(a)

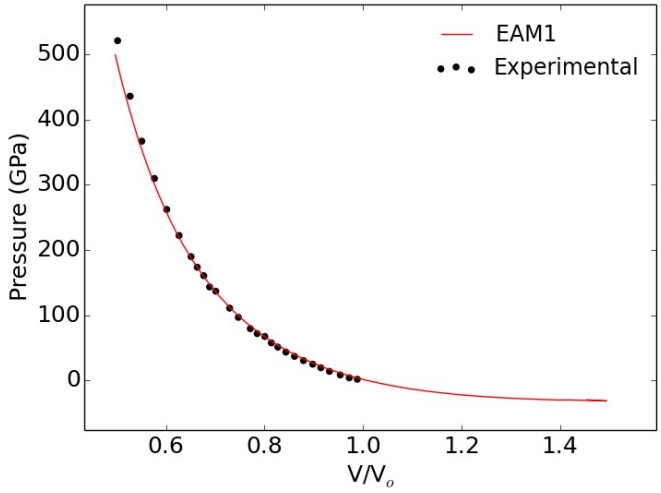

(b)

Figure 3.2: (a) The cold curve of Tantalum, calculated with the embedded atom potential Ta2 [5]. Note: Equilibrium volume $V = 18.034\dot{A}^3$; $P(V, 0) = -0.79$ GPa. (b) Pressure volume relation at zero temperature (cold) for Tantalum calculated with the embedded atom potential Ta 2 [5]. These results are compared with experimental data [7] [8].

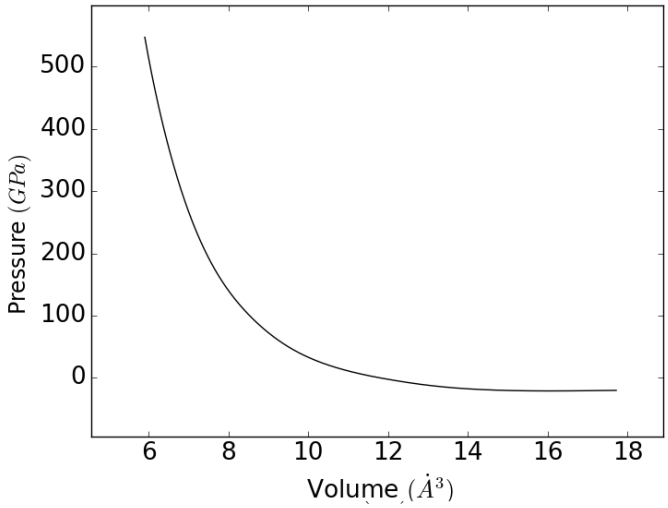

(a)

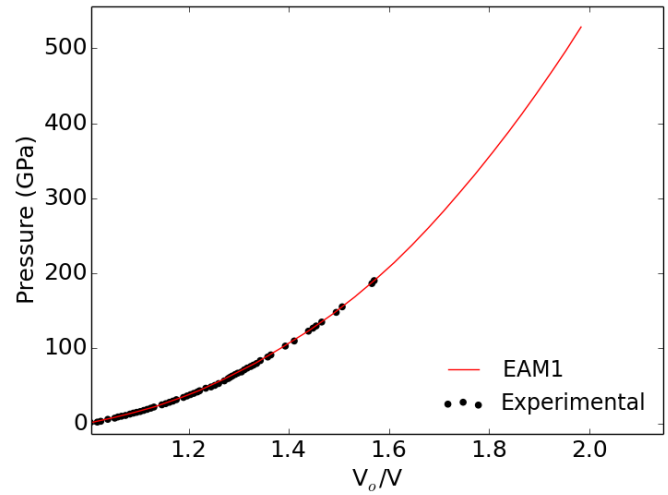

(b)

Figure 3.3: (a) The cold curve of Copper, calculated with the embedded atom potential EAM1 [6]. Note: Equilibrium volume $V = 11.810\dot{A}^3$; $P(V, 0) = -1.91$ GPa. (b) Pressure volume relation at zero temperature (cold) for Copper calculated with the embedded atom potential EAM 1 [6]. These results are compared with experimental data [9] [10].

Chapter 4

Molecular Dynamics Simulations

In this chapter we present the atomistic simulations and their results for Tantalum and Copper. The MD simulations for these metals predict the variation of the Gruneisen parameters' value with increasing constant pressure. It was of interest to study the effect of pressure on the behavior of the Gruneisen parameter over a wide temperature regime. The effects of increasing pressure on the linear thermal expansion coefficient are also shown.

4.1 Virtual Atomic Crystals

A virtual crystal represents the isolated system of atoms in the MD simulations. By specifying the type and N number of atoms, among other parameters, it is possible to simulate a crystalline material of any size. Note that the number of atoms will affect the economy of the simulations as the size of the problem can cause difficulties in terms of numerical formulations.

Ta and Cu crystals arranged in body-center-cubic (BCC) and face-center-cubic (FCC) unit cells, respectively, are shown in Figures 4.1. Note that for this work the atoms are arranged to form an overall cubic structure. These crystals were thermalized to a temperature of 0 K to provide the simulation with an initial configuration.

Table 4.1: Some parameters of the Tantalum virtual crystal. Initial crystal parameter values are shown as are the resulting values after thermalizing the crystal to 0 K. Note: a_0 = lattice constant; V = volume; ρ = density.

	Value	Thermalized (0 K)	T = 300 K
$a_0(\dot{A})$	3.304	3.304	3.309
$V(\dot{A}^3)$	18.034	18.034	18.111
$\rho(\dot{A}^{-3})$	0.0554	0.0554	0.0552

Table 4.2: Some parameters of the Copper virtual crystal. Initial crystal parameter values are shown as well as resulting values after thermalizing the crystal to 0 and 300 K. Note: a_0 = lattice constant; V = volume; ρ = density.

	Value	Thermalized (0 K)	T = 300 K
$a_0(\dot{A})$	3.615	3.615	3.632
$V(\dot{A}^3)$	11.809	11.810	11.976
$\rho(\dot{A}^{-3})$	0.0847	0.0847	0.0835

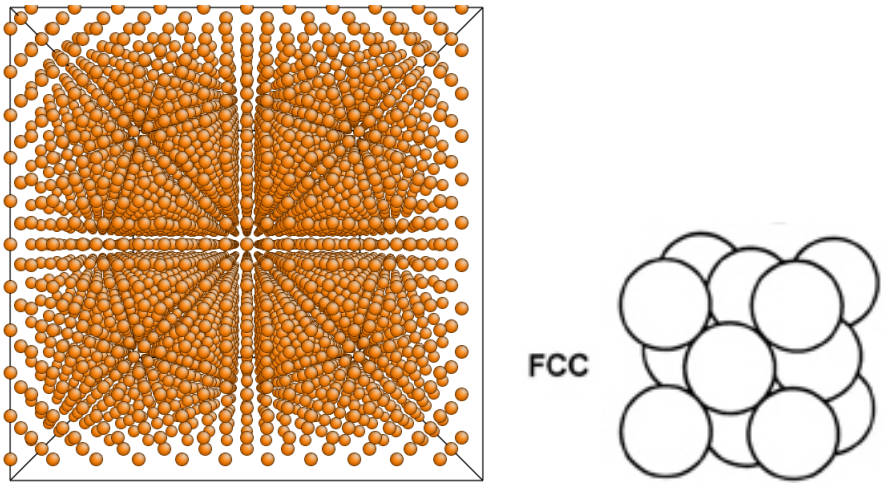

(a) Cu Virtual Crystal

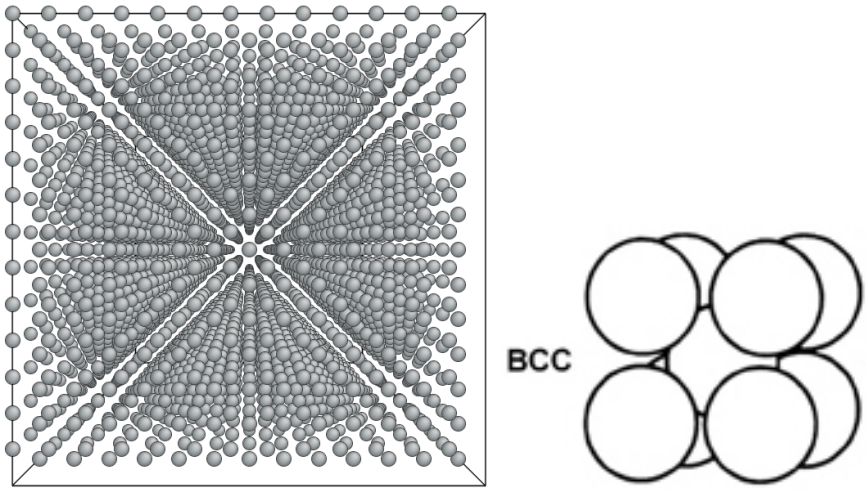

(b) Ta Virtual Crystal

Figure 4.1: Perspective 3-dimensional view of the virtual crystals and the respective unit cell diagram. Atomic size not to scale. (a) Face-centered cubic (FCC) arrangement of 5324 Copper atoms with lattice constant $a_0 = 3.615\ \dot{A}$. (b) Body-centered cubic (BCC) arrangement of 4394 Tantalum atoms with lattice constant $a_0 = 3.304\ \dot{A}$.

4.2 Material Simulations

The MD simulations were performed with the use of each materials thermalized crystal and the corresponding potential. The simulations for Ta were performed for a temperature range of 30 to 2200 K. Simulations for Cu were performed for the temperature range of 30 to 1500 K. The difference in each upper temperature limit stemmed from wanting to keep the simulations below each materials melt temperature while still exploring a large temperature regime. These simulations were isobaric: at constant zero pressure and at a higher constant pressure of 10 GPa. MD results for the given pressure-energy relations are shown in Figures 4.2 for Ta and 4.3 for Cu.

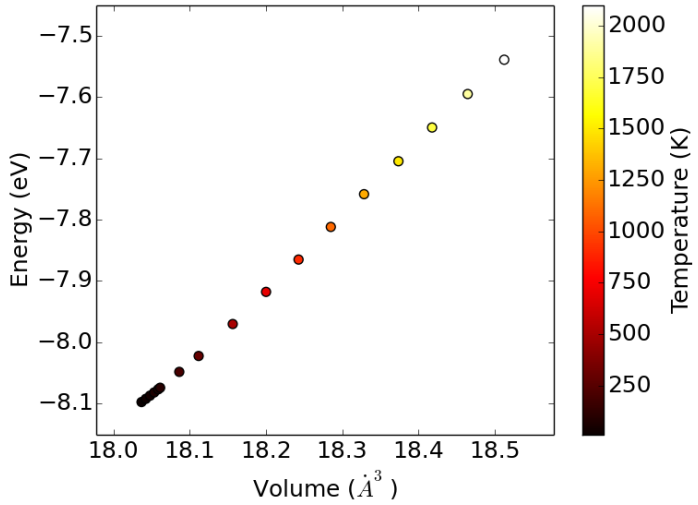

(a)

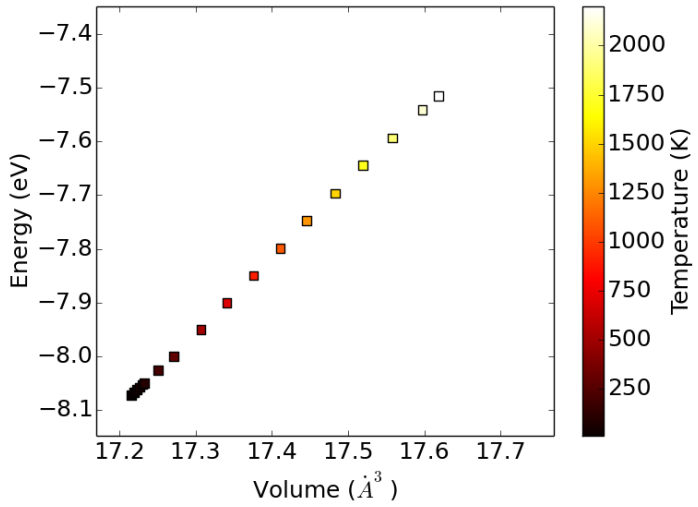

(b)

Figure 4.2: Pressure-energy relation from molecular dynamics simulations of Tantalum. Simulations were performed at constant pressure: (a) Zero pressure, (b) 10 GPa. The corresponding temperature change is shown with a colored bar.

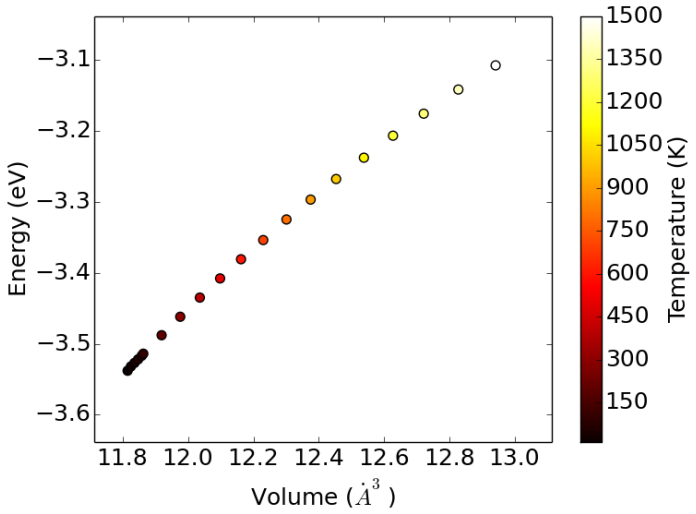

(a)

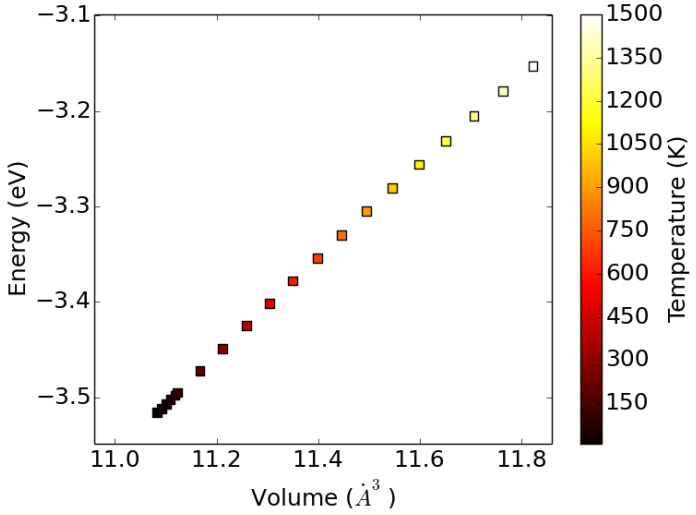

(b)

Figure 4.3: Pressure-energy relation from molecular dynamics simulations of Copper. Simulations were performed at constant pressure: (a) Zero pressure, (b) 10 GPa. The corresponding temperature change is shown with a colored bar.

4.3 Gruneisen Parameter Calculations

The isobaric γ was calculated with the use of the previously mentioned equation:

$$\gamma = V(\frac{\partial P}{\partial E})_V \tag{4.1}$$

Note that equation (4.1) works under constant volume, while the interests of this work was to study γs' behavior with increasing constant pressure. For this reason MD simulations at constant pressure were performed first. The resulting isobaric volumes were then used to run small simulation sets at constant volume. These isometric MD simulations kept the isobaric volumes constant for a short temperature range. This range was chosen slightly over and below the original temperature corresponding to each isobaric volume, e.g., an isobaric simulation volume corresponding to a temperature of 30 GPa would be used to perform isometric simulations at 25 and 35 GPa. The Gruneisen parameter was then calculated as the slope of each of these isometric pressure-energy data sets.

The isobaric simulations were performed at 0, 5, and 10 GPa. However, here only results for 0 and 10 GPa are shown. The results from the isobaric MD simulations are shown in Figures 4.4 and 4.6. As expected, the volume sets at higher pressure are lower than the zero pressure values. The Gruneisen parameter results as a function of temperature can be seen in Figures 4.4b and 4.6b.

The results for the linear thermal expansion α, at constant pressure, can be seen in Figures 4.5 and 4.7. These values were calculated with the use of the following equation:

$$\alpha = \frac{1}{3V_0}(\frac{\partial V}{\partial T})_P \tag{4.2}$$

The volume-temperature relations were fit to a quadratic line. This ensured a linear first derivative, which helped to view the effects of pressure clearly. More accurate results for α can be seen in Chapter 6.

With the use of an approximation for isotropic solids, $\alpha = \beta/3$, and the relation $(\frac{\partial P}{\partial T})_V = \beta B_0$ equation (4.1) becomes:

$$\gamma_2 = (\frac{3\alpha B_0 V}{C_V}) \tag{4.3}$$

This equation was used along with MD results for α to calculate γ_2 and compare to the true γ results at 0 and 10 GPa. The zero pressure results for Ta can be seen in Figure 4.8a. Results for Cu at zero pressure can be seen in Figures 4.9a. It was also of interest to see what effect pressure had on these equations agreement. The results at a constant pressure of 10 GPa can be seen for Ta and Cu in Figures 4.8b and 4.9b, respectively.

Equations (4.1) and (4.3) should yield comparable results in order for their thermodynamic equivalency to hold true. This however does not seem to be the case for all temperatures. Generally speaking, zero-pressure calculations of γ_2 at high temperatures seems to be an overestimate. The increase from a constant pressure of 0 to 10 GPa appears to reduce the range of both γ and γ_2 values. This higher pressure also pushes the starting point for γ_2 as an overestimation to a higher temperature. The overestimation of γ_2 at high temperatures could be attributed to the equation not accounting for the softening or decrease of B_T with temperature. Note that equation (4.1) does account for this change in B_T.

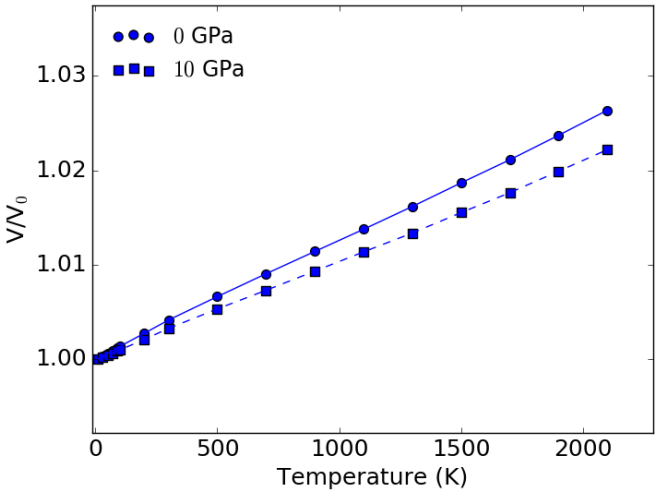

(a)

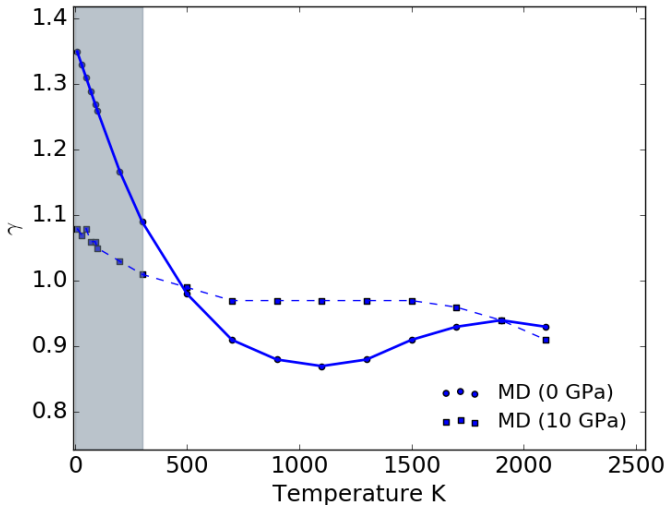

(b)

Figure 4.4: Calculations from molecular dynamics simulations. (a) Volume-temperature relation of Tantalum from isobaric molecular dynamics simulations at 0 and 10 GPa. Note: V/V_0 = Fractional change in volume. (b) Isobaric Gruneisen parameter of Tantalum calculated using molecular dynamics. Constant pressure values of 0 and 10 GPa. The are below the materials Debye temperature is shown in gray ($T_D = 246$ K).

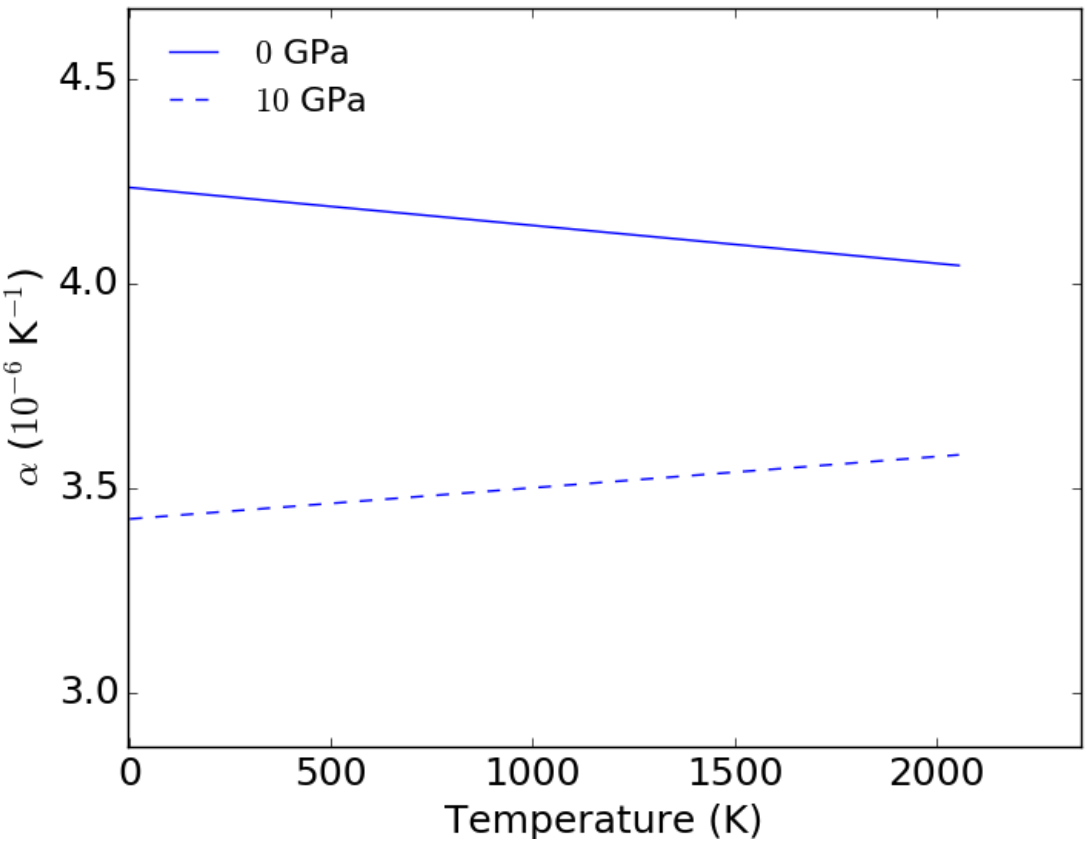

Figure 4.5: Thermal linear expansion-temperature relation of Tantalum from isobaric molecular dynamics simulations. Constant pressure values of 0 and 10 GPa. Note: Thermal linear expansion calculated from a quadratic fit to the original isobaric volume results.

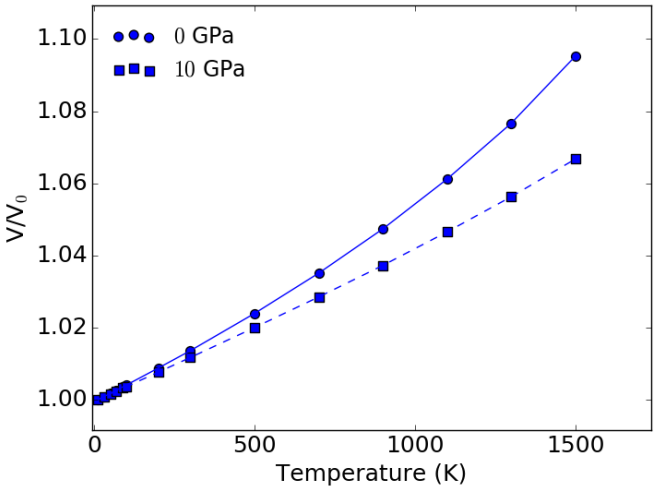

(a)

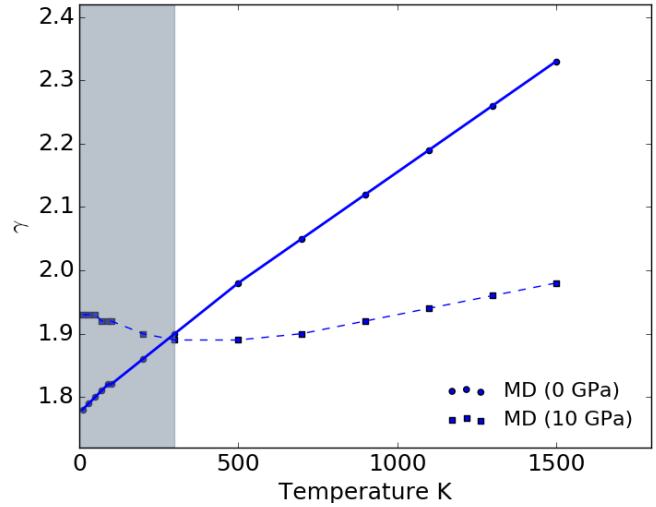

(b)

Figure 4.6: Calculations from molecular dynamics simulations. (a) Volume-temperature relation of Copper from isobaric molecular dynamics simulations at 0 and 10 GPa. Note: V/V_0 = Fractional change in volume. (b) Isobaric Gruneisen parameter of Copper calculated using molecular dynamics. Constant pressure values of 0 and 10 GPa. The are below the materials Debye temperature is shown in gray ($T_D = 347$ K).

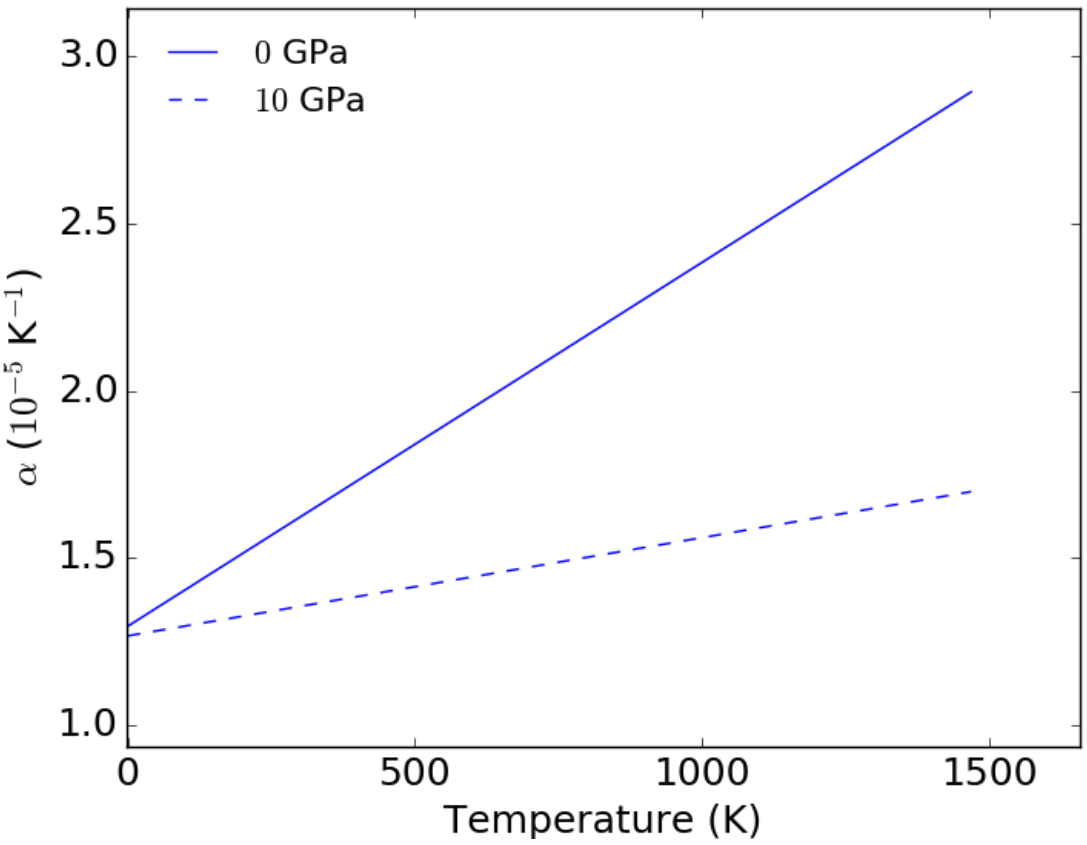

Figure 4.7: Thermal linear expansion-temperature relation of Copper from isobaric molecular dynamics simulations. Constant pressure values of 0 and 10 GPa. Note: Thermal linear expansion calculated from a quadratic fit to the original isobaric volume results.

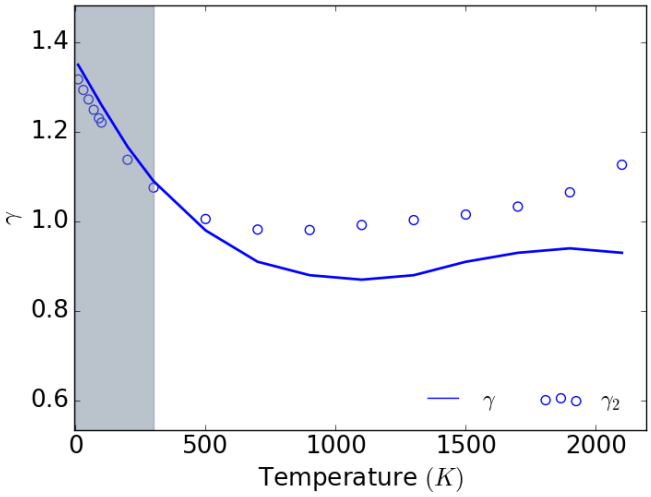

(a)

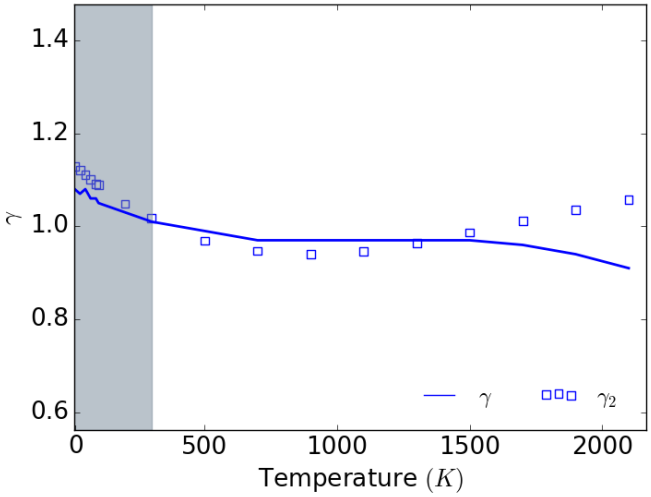

(b)

Figure 4.8: Comparison of Gruneisen Parameter equations for Tantalum at the constant pressure. The are below the materials Debye temperature is shown in gray ($T_D = 246$ K). (a) Constant pressure of 0 GPa. The solid line represents results from MD simulations where $\gamma = V(\frac{\partial P}{\partial E})_V$. The circle markers represents results from the equation which assumes $(\frac{\partial P}{\partial T})_V = \beta B_0$. (b) Constant pressure of 10 GPa. The solid line represents results from MD simulations where $\gamma = V(\frac{\partial P}{\partial E})_V$. The square markers represents results from the equation which assumes $(\frac{\partial P}{\partial T})_V = \beta B_0$.

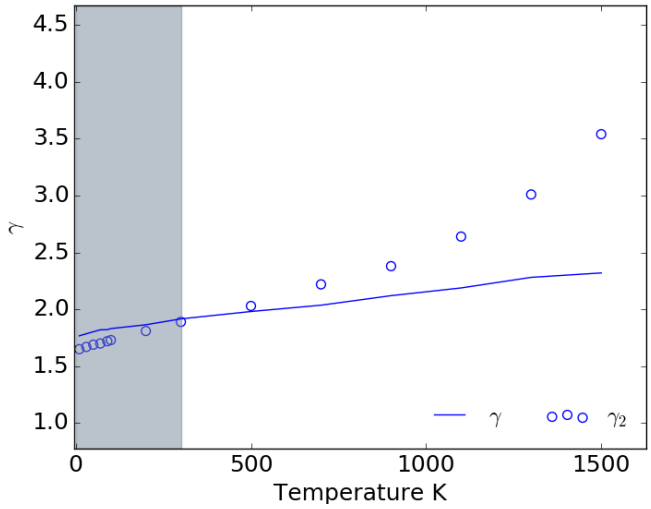

(a)

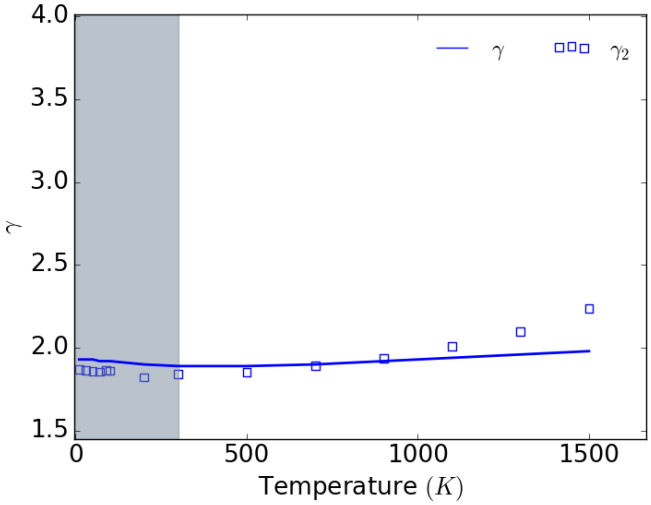

(b)

Figure 4.9: Comparison of the Gruneisen Parameter equations for Copper at the constant pressure. The are below the materials Debye temperature is shown in gray ($T_D = 347$ K). (a) Constant pressure of 0 GPa. The solid line represents results from MD simulations where $\gamma = V(\frac{\partial P}{\partial E})_V$. The circle markers represents results from the equation which assumes $(\frac{\partial P}{\partial T})_V = \beta B_0$. (b) Constant pressure of 10 GPa. The solid line represents results from MD simulations where $\gamma = V(\frac{\partial P}{\partial E})_V$. The square markers represents results from the equation which assumes $(\frac{\partial P}{\partial T})_V = \beta B_0$.

Chapter 5

Calculations from Gruneisen Parameter Models

In this chapter we present results for models of the Gruneisen parameter in Tantalum and Copper. These include the following: The Mie-Gruneisen EoS parameter; The Slater Gruneisen parameter, The Dugdale-MacDonald Gruneisen parameter; The Vashchenko-Zubarev Gruneisen parameter; and The Vibrational Gruneisen parameter. It was of interest to compare these with the isobaric results for γ shown in Chapter 4.

5.1 The Mie-Gruneisen Parameter

As previously mentioned, isolating γ from the original Mie-Gruneisen EoS gives:

$$\gamma_{EoS} = \frac{[P(V,T) - P(V,0)]V}{C_V T} \tag{5.1}$$

The cold energy and cold pressure of the materials, Ta and Cu, were calculated first during the evaluation of the embedded atom potentials. The equilibrium volume used for Ta was 18.034 $\dot{A}^3$. The resulting cold curve of Ta can be seen again in Figure 3.2a. For Cu, the equilibrium volume used was 11.810 $\dot{A}^3$.The cold curve of Cu can be seen in Figure 3.3a. The interest in these cold curves for calculating γ_{EoS} was to find the cold pressure $P(V,0)$ corresponding to each materials equilibrium volume. The behavior of γ_{EoS} over each materials temperature regime are shown in Figures 5.1 and 5.2.

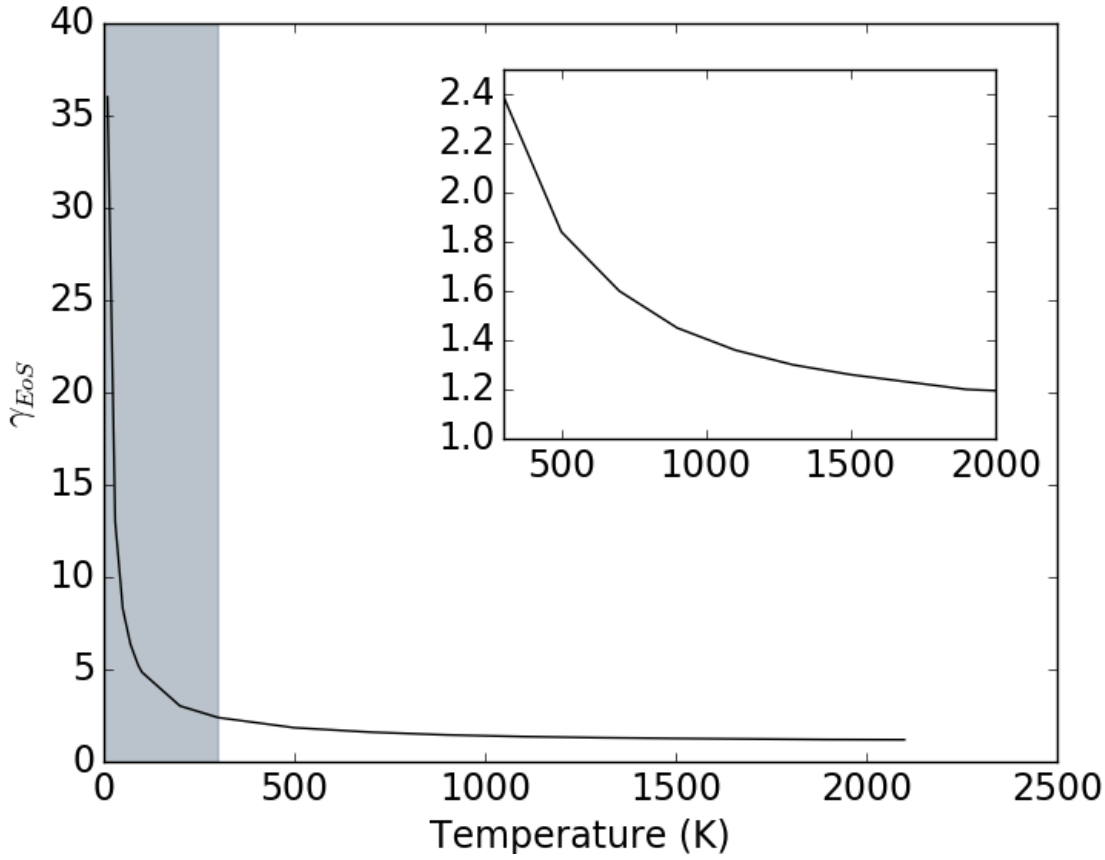

Figure 5.1: Mie-Gruneisen parameter of Tantalum. The are below the materials Debye temperature is shown in gray ($T_D = 246$ K). A zoom subplot is included to better display high temperature behavior. Note: Equilibrium volume= 18.034 $\dot{A}^3$.

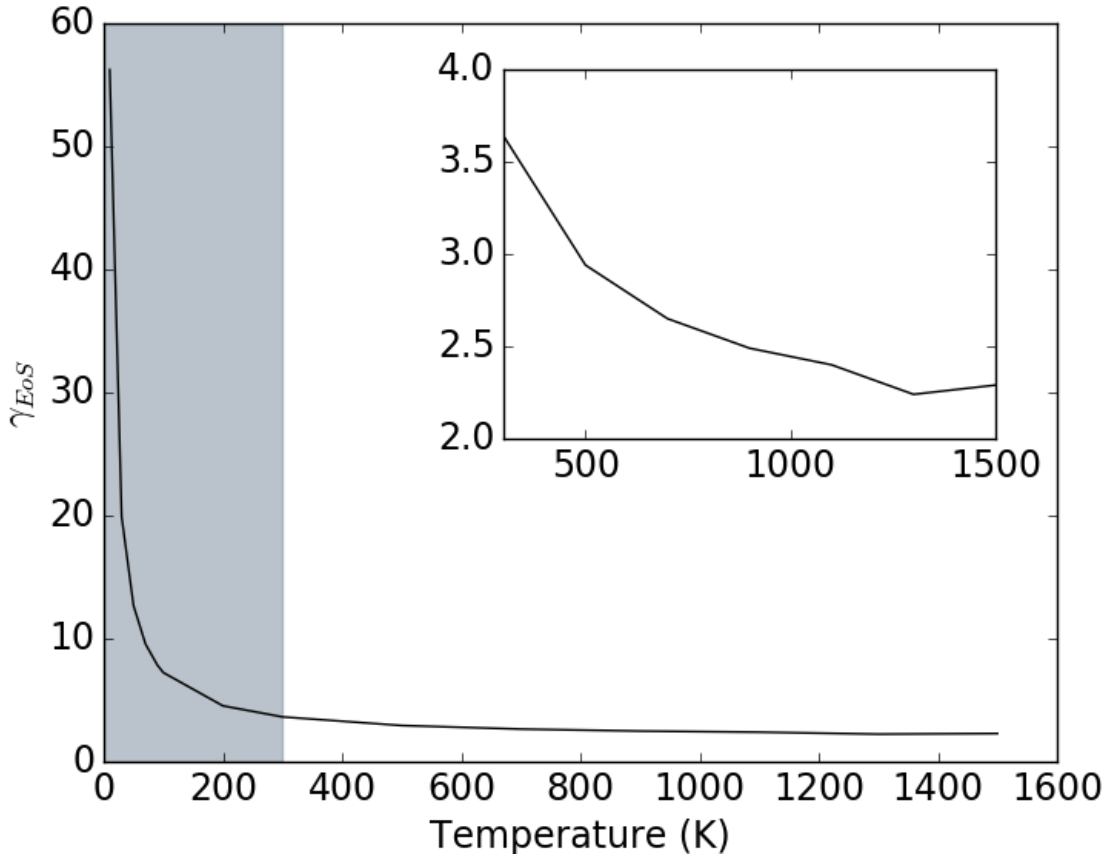

Figure 5.2: Mie-Gruneisen parameter of Copper. The are below the materials Debye temperature is shown in gray ($T_D = 347$ K). A zoom subplot is included to better display high temperature behavior. Note: Equilibrium volume= 11.810 $\dot{A}^3$.

5.2 Mechanical Gruneisen Models

As seen in Chapter 2, several other macroscopic definitions of the Gruneisen Parameter were developed based on derivatives of the cold curve. Some previously mentioned definitions are the Slater model γ_S, the Dugdale-MacDonald model γ_{DM},and the Vashchenko-Zubarev model γ_{VZ}. The definition of γ_S at zero pressure is again written as:

$$\gamma_S = \frac{1}{2}B_0' - \frac{1}{6} \tag{5.2}$$

The Dugdale-MacDonald model has been known to fit a wide spectrum of materials and is simply described with respect to the bulk modulus fist derivative at P=T=0 as [11]:

$$\gamma_{DM} = \frac{1}{2}B_0' - \frac{1}{2} \tag{5.3}$$

Equation (5.3) is known to have limitations [4]. It was later improved on by the Vashchenko-Zubarev model. To better capture anharmonicity γ_{VZ} considered three-dimensional oscillations as oppose to the simplified one-dimensional harmonic oscillations of γ_{DM}. This model at zero pressure is written as:

$$\gamma_{VZ} = \frac{1}{2}B_0' - \frac{5}{6} \tag{5.4}$$

Results using these models were calculated at zero pressure from the values of B_0 and B'. These models as a function of temperature can be seen in Figures 5.5 and 5.6 for Ta and Cu, respectively. Because these models require experimental data for B' the values from the MD simulation at zero pressure were used. This helped to better compare γ_S, γ_{DM}, and γ_{VZ} to γ in following chapters.

Table 5.1: The Gruneisen parameter, γ, of various materials. The values vary depending on the definition use. Note: γ = Thermodynamic definition; γ_S = Slater definition; γ_{DM} = Dugdale-MacDonald definition; γ_{VZ} = Vashchenko-Zubarev definition.

Material (0 GPa pressure at 300 K)	γ	γ_S	γ_{DM}	γ_{VZ}	B_0 (GPa)	B'
Cu	1.92	1.19	0.52	0.19	135.35	2.04
Ta	1.89	1.83	1.48	1.13	192.89	3.96

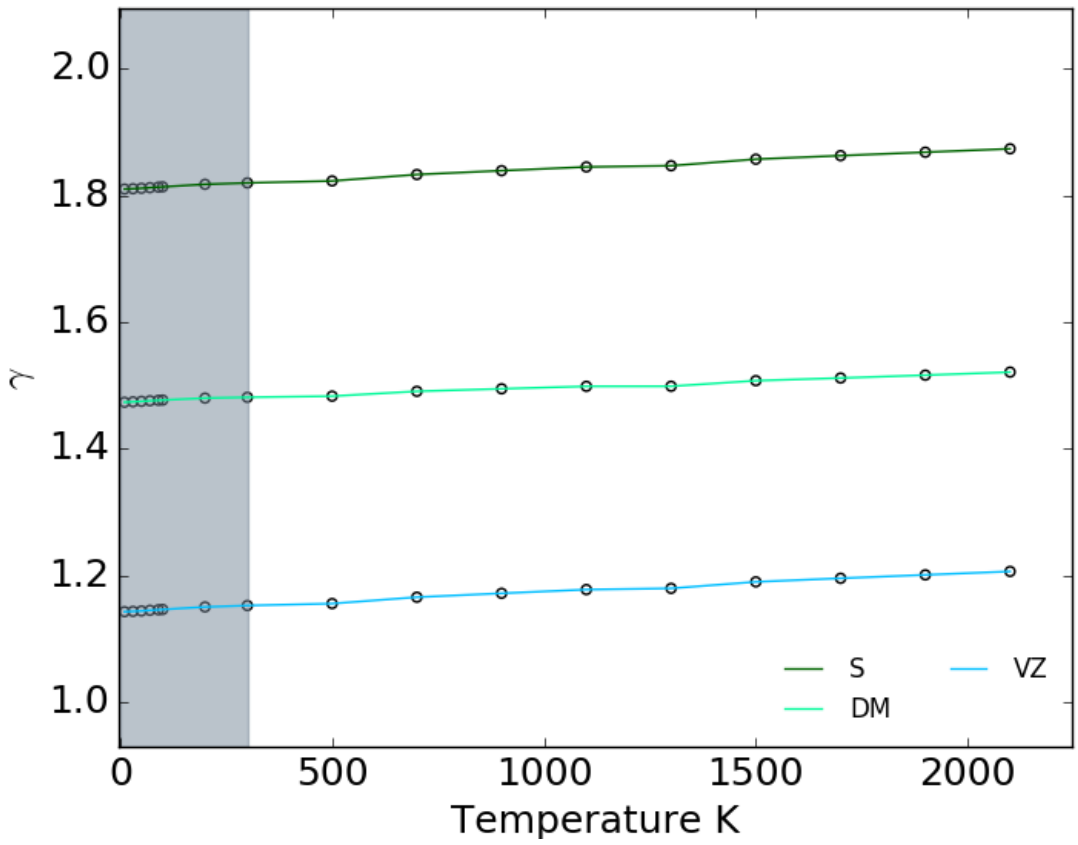

Figure 5.3: The Slater (dark green), Dugdale-MacDonald (light green), and the Vashchenko-Zubarev (light blue) Gruneisen parameters model calculations for Tantalum at zero pressure. The area below 300 K for the material is shown in gray (Debye temperature =246 K).

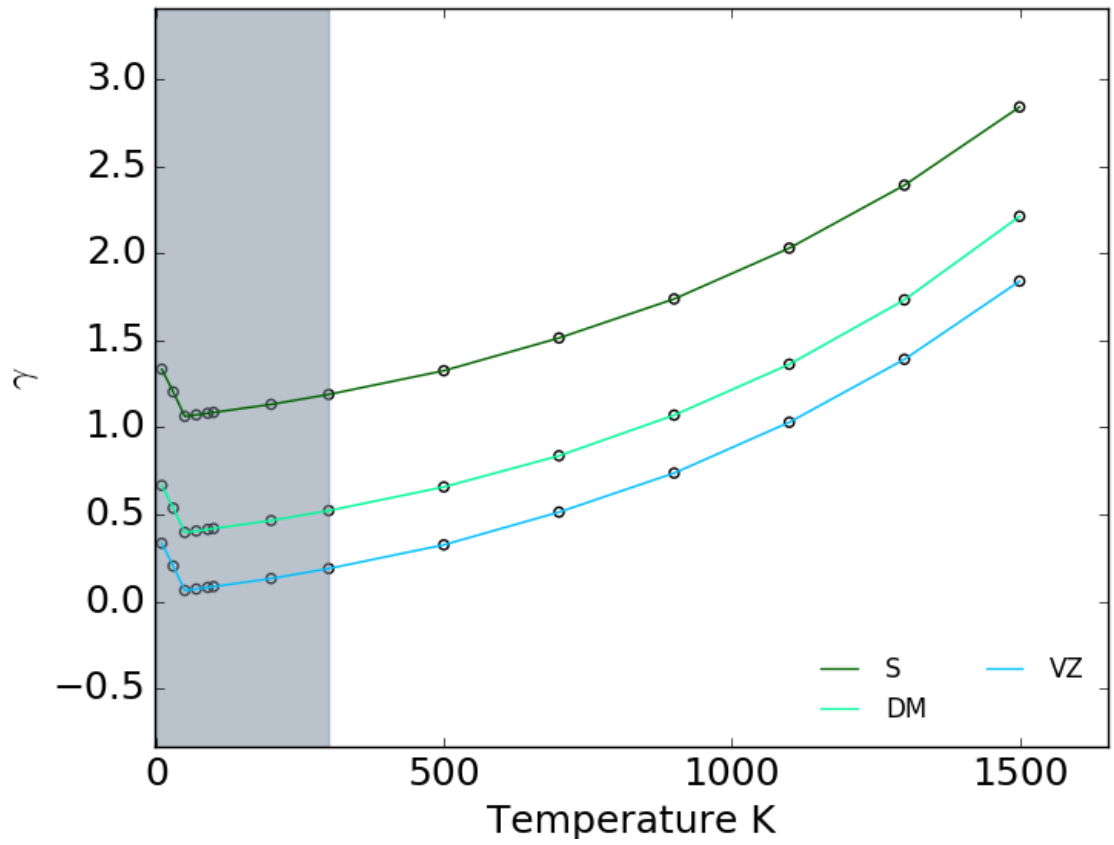

Figure 5.4: The Slater (dark green), Dugdale-MacDonald (light green), and the Vashchenko-Zubarev (light blue) Gruneisen parameters model calculations for Copper at zero pressure. The area below 300 K for the material is shown in gray (Debye temperature =347 K).

Since these are all improvements on γ_S, at non zero pressures it is possible to focus on the more relevant mechanical models γ_{DM}, and γ_{VZ}. The models γ_{DM} and γ_{VZ} are written for non zero pressures as:

$$\gamma(V) = \frac{[\frac{B'}{2} - \frac{1}{6} - \frac{t}{3}](1 - \frac{P}{3B_T})}{[1 - \frac{2t}{3}\frac{P}{B_T}]} \begin{cases} t = 1 & (\gamma_{DM}) \\ t = 2 & (\gamma_{VZ}) \end{cases} \tag{5.5}$$

Tables 5.1 and 5.2 show results for Ta and Cu at 300 K for reference. Results at all the temperatures in the regime for Ta for 10 GPa are shown in Figure 5.5. For Cu, results at all the temperatures in the regime for 10 GPa are shown in Figure 5.6.

Table 5.2: The Gruneisen parameter, γ, of various materials. The values vary depending on the definition use. Note: γ = Thermodynamic definition; γ_S = Slater definition; γ_{DM} = Dugdale-MacDonald definition; γ_{VZ} = Vashchenko-Zubarev definition.

Material (10 GPa pressure at 300 K)	γ	γ_{DM}	γ_{VZ}	B_0 (GPa)	B’
Cu	1.89	1.63	1.43	165.70	4.2671
Ta	1.02	1.41	1.15	228.29	3.81

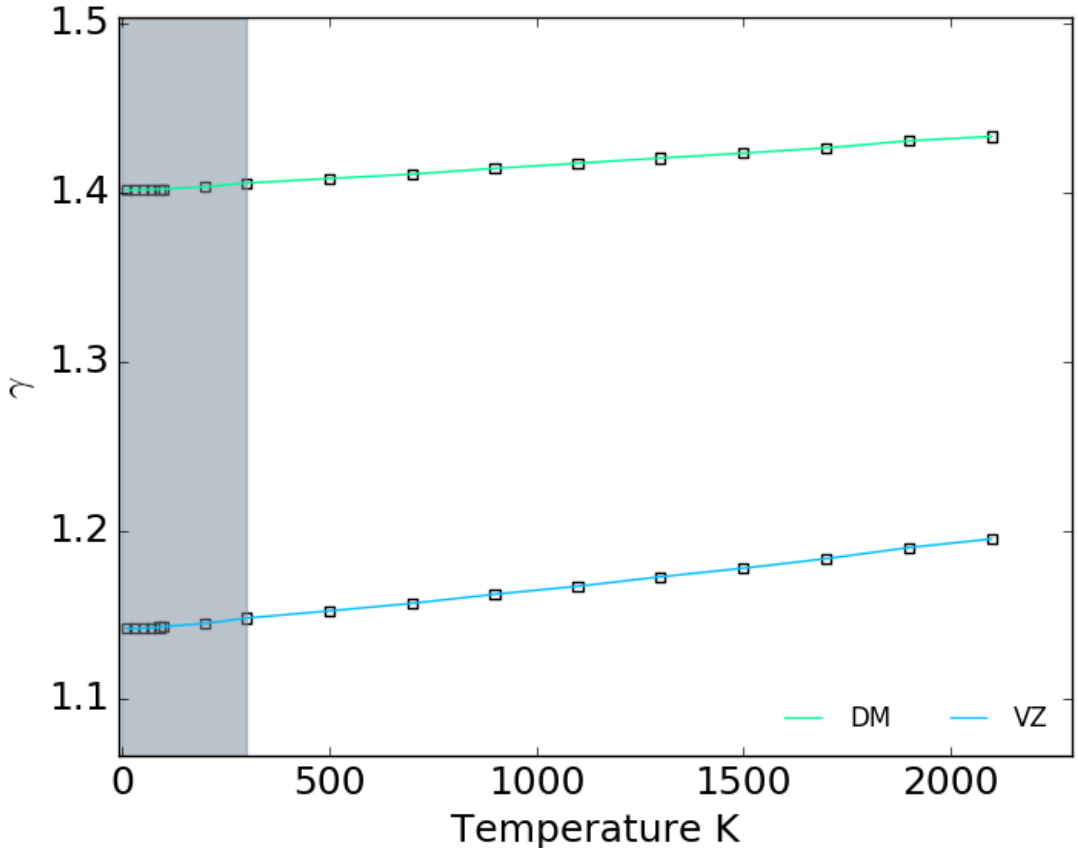

Figure 5.5: The Dugdale-MacDonald (light green), and the Vashchenko-Zubarev (light blue) Gruneisen parameters model calculations for Tantalum at a constant pressure of 10 GPa. The area below 300 K for the material is shown in gray (Debye temperature =246 K).

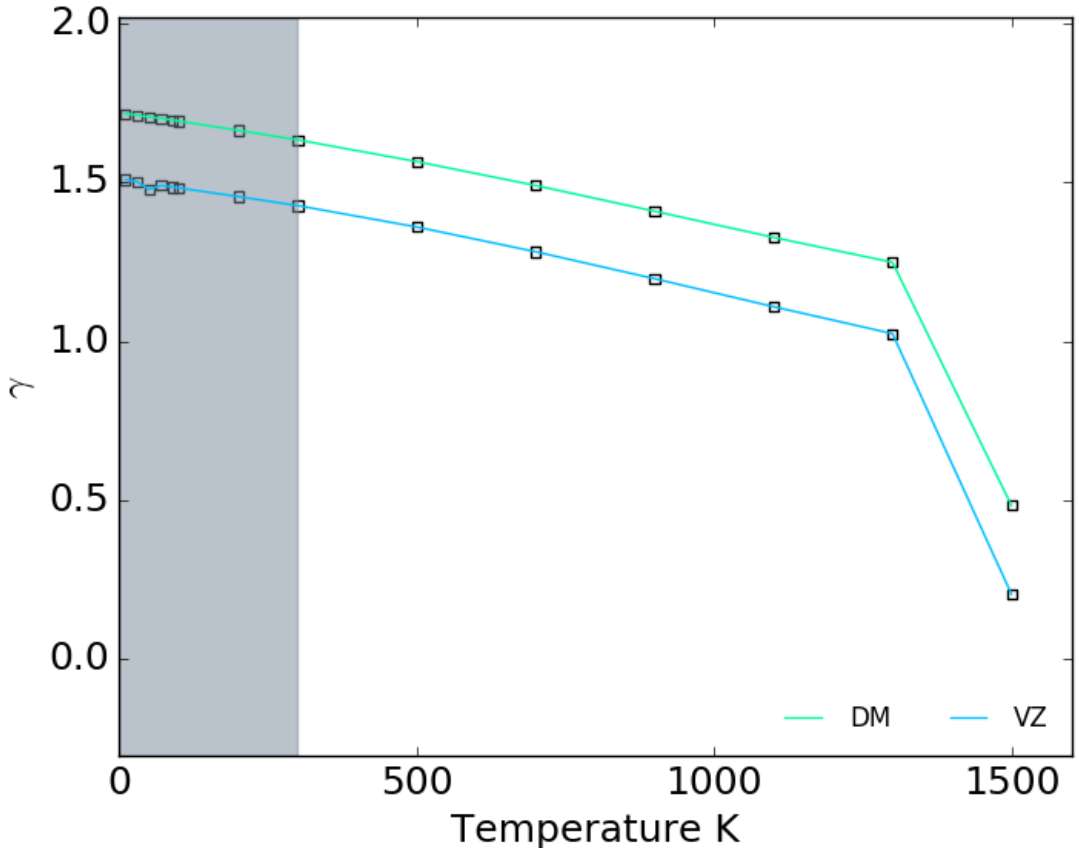

Figure 5.6: The Dugdale-MacDonald (light green), and the Vashchenko-Zubarev (light blue) Gruneisen parameters model calculations for Copper at a constant pressure of 10 GPa. The area below 300 K for the material is shown in gray (Debye temperature =347 K).

5.3 Vibrational Gruneisen Model

The classical vibrational Gruneisen parameter, noted as γ_{Vib}, was calculated. In order to compare γ_{Vib} and γ a range of temperature-equivalent volumes from the MD results were needed, due to γ_{Vib} being temperature independence. The volumes from the MD simulations at constant pressure (0, 5, 10 GPa) were used. The relational behavior of volume and γ_{Vib} for Ta and Cu can be seen in Figures 5.7 and 5.8, respectively. The temperatures corresponding each MD volume are depicted with the help of a temperature bar.

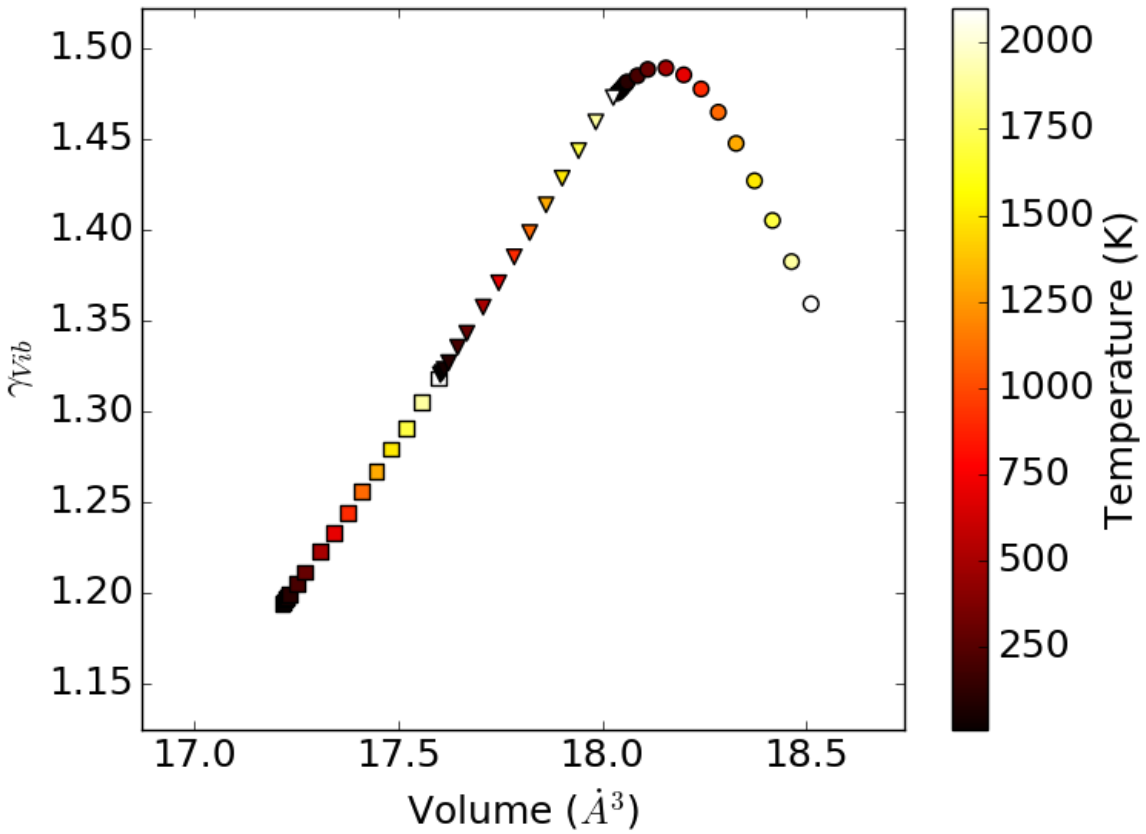

Figure 5.7: Relation of the vibrational Gruneisen parameter γ_{Vib}, and volume for Tantalum. Calculated in the quasi-harmonic approximation at various constant pressures. Note that γ_{Vib} was calculated from a set of molecular dynamics temperature equivalent volumes. Marker labels: $\bigcirc = 0$ GPa; $\bigtriangledown = 5$ GPa; $\square = 10$ GPa.

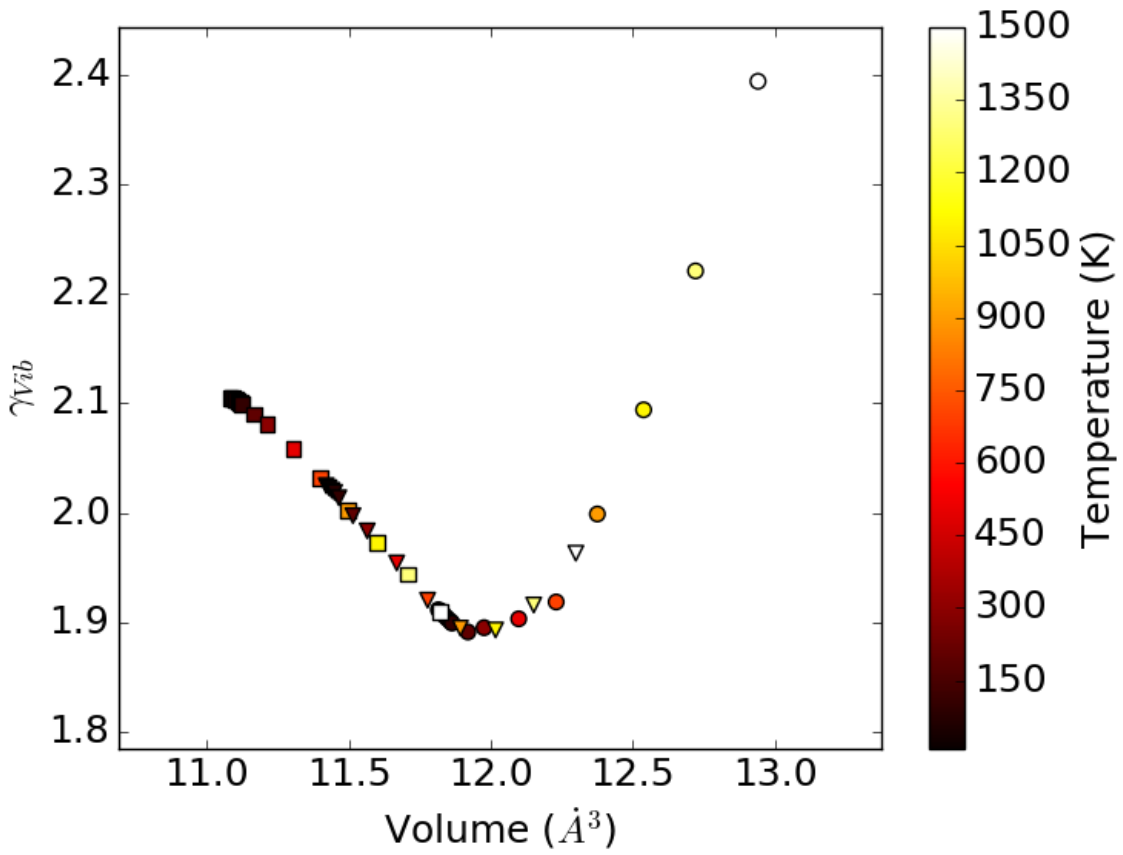

Figure 5.8: Relation of the vibrational Gruneisen parameter γ_{Vib}, and volume for Copper. Calculated in the quasi-harmonic approximation at various constant pressures. Note that γ_{Vib} was calculated from a set of molecular dynamics temperature equivalent volumes. Marker labels: $\bigcirc = 0$ GPa; $\bigtriangledown = 5$ GPa; $\square = 10$ GPa.

Chapter 6

Discussion

Over all, this work finds Gruneisen parameter models are inconsistent. The temperature contribution to γ (and by proxy anharmonicity) is more significant than previously believed. This can be seen most clearly from the misses by models focused on the bulk modulus and its derivative with respect temperature. Mechanical models show significant disagreement with MD results for γ for both material examples. This means that measurements solely based on experimental B_0 and B' values should not be expected to reproduce correct results for γ in other materials.

At the start of this work the quasi-harmonic approximation model was selected as it provides information on how γ changes with pressure. QHA performed well for some calculations. Linear expansion calculations effectively reproduce α behavior over temperature particularly below 300 K. However, the classical limit γ_{Vib} shows inconsistent results among the material examples. While not perfect, γ_{Vib} matches γ results for Cu better than for Ta. It is yet to be determined why this is the case, but do note that there can be no expectation that models like QHA (not inclusive of temperature) will reproduce the correct γ and thermal pressure of more complex materials.

The increase in pressure from 0 GPa to 10 GPa shows interesting results. There is a notable effect on the range and slope. This decrease in range and flattening of the slope is also seen when increasing pressure on γ_{Vib} calculations. This pressure change appears to have an effect on the thermal equivalency of equations (4.1) and (4.3). While both equations show the fore mentioned effects the zero pressure agreement seen at low temperatures is diminished at the higher pressure.

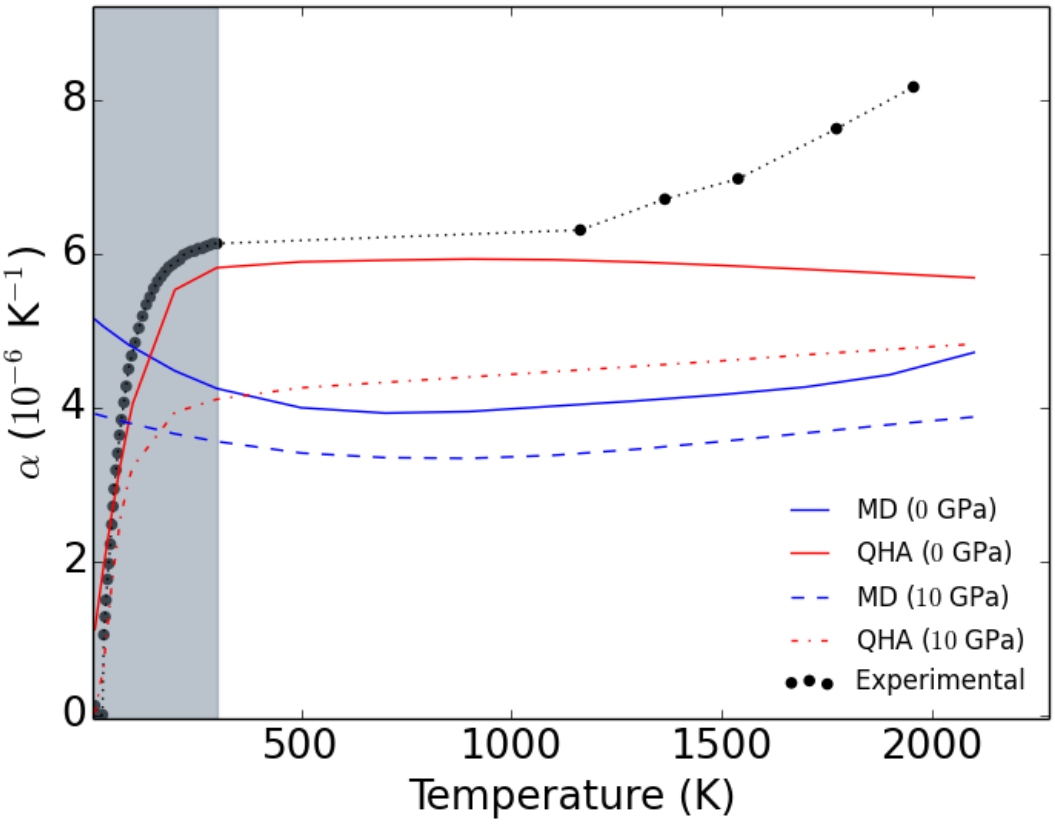

Figure 6.1: Comparison between thermal linear expansion coefficients of Tantalum calculated from molecular dynamics and the quasi-harmonic approximation at 0 and 10 GPa. The true definition α is shown in blue. Results calculated from the vibrational Gruneisen parameter are shown in red, α_{Vib}. The black circle markers shows experimental data included for comparison [2]. Note the region below the Debye temperature is shown in gray.

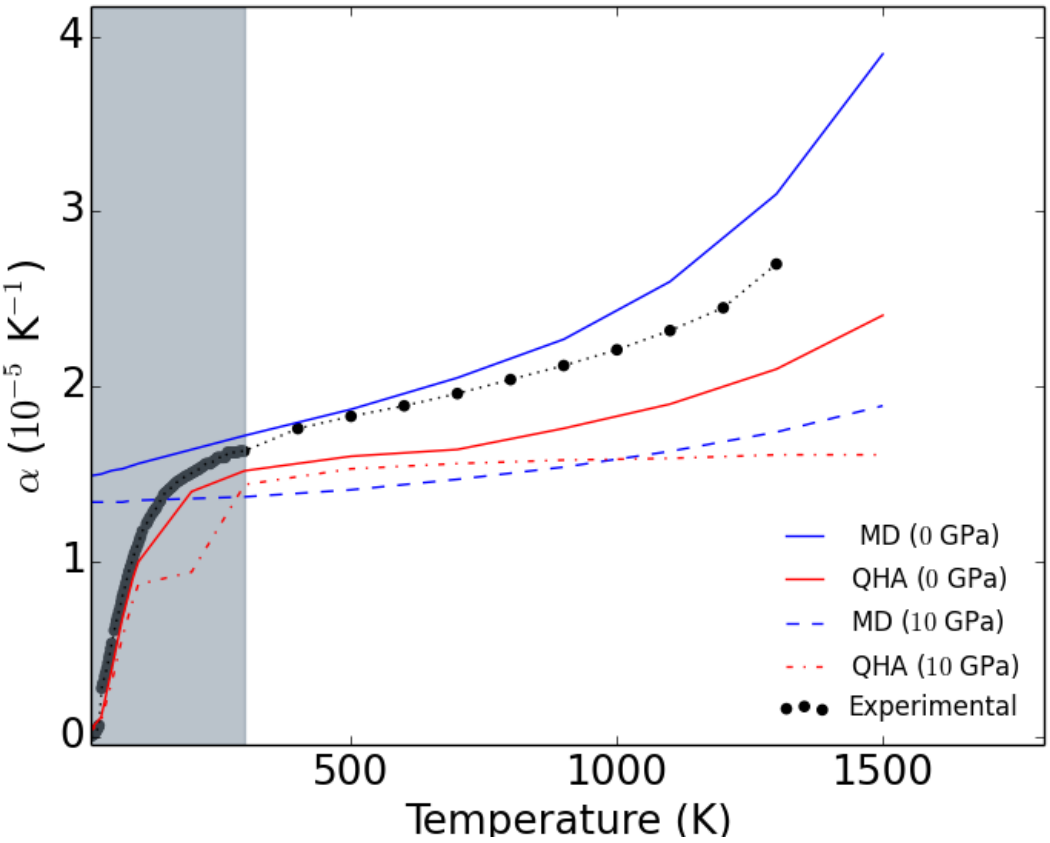

Figure 6.2: Comparison between thermal linear expansion coefficients of Copper calculated from molecular dynamics and the quasi-harmonic approximation at 0 and 10 GPa. The true definition α is shown in blue. Results calculated from the vibrational Gruneisen parameter are shown in red, α_{Vib}. The black circle markers shows experimental data included for comparison [2]. Note the region below the Debye temperature is shown in gray.

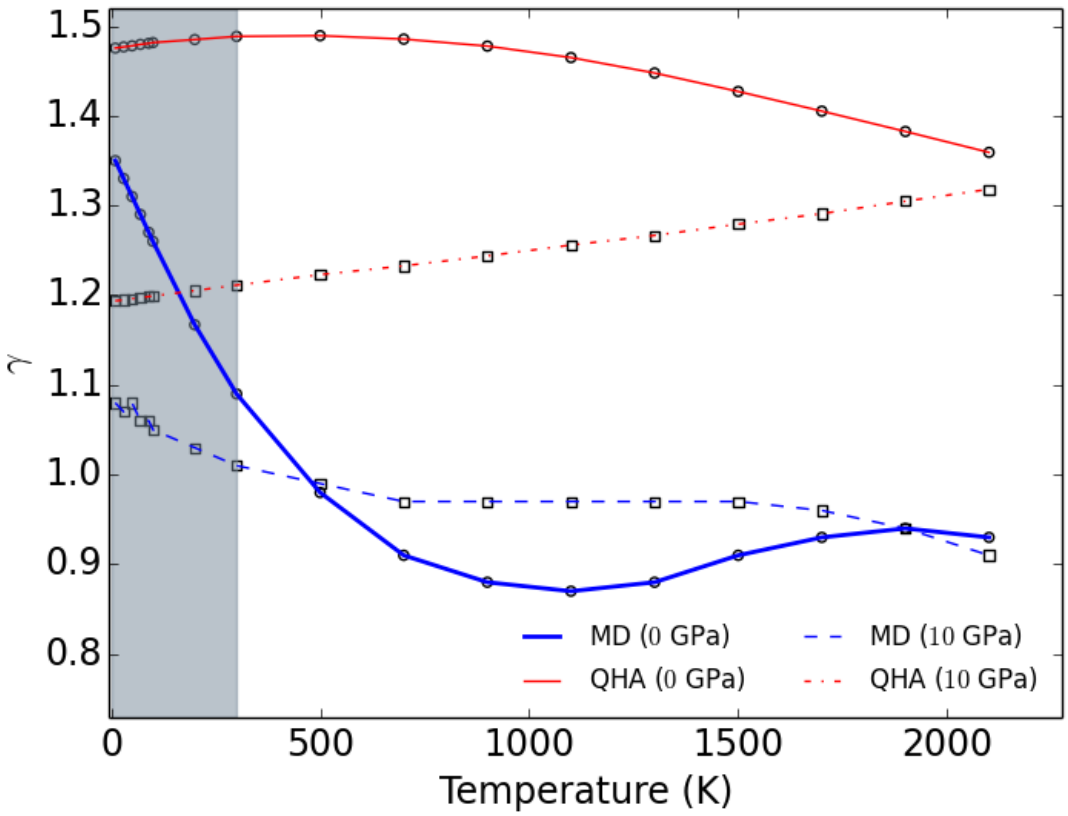

Figure 6.3: Comparison of the Gruneisen parameter (blue) and the Vibrational Gruneisen parameter (classical limit, red) of Tantalum. Isobaric calculations at 0 and 10 GPa. Note the region below the Debye temperature is shown in gray.

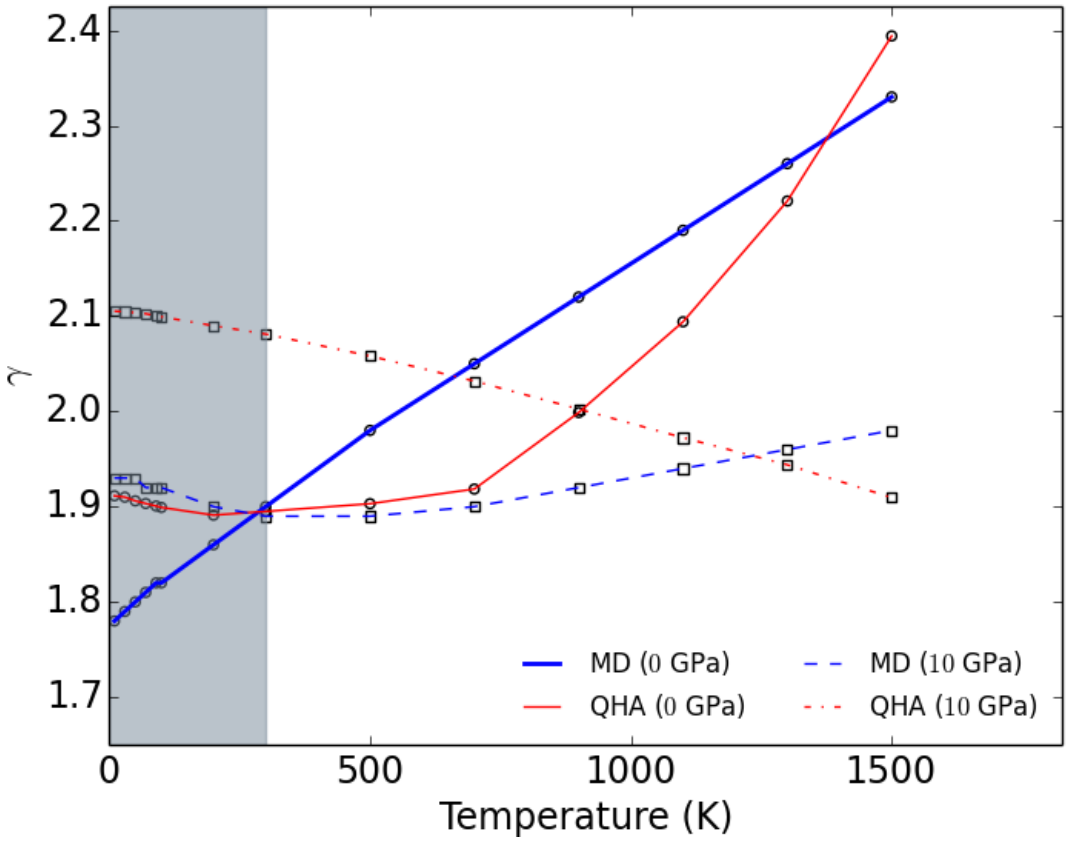

Figure 6.4: Comparison of the Gruneisen parameter (blue) and the Vibrational Gruneisen parameter (classical limit, red) of Copper. Isobaric calculations at 0 and 10 GPa. Note the region below the Debye temperature is shown in gray.

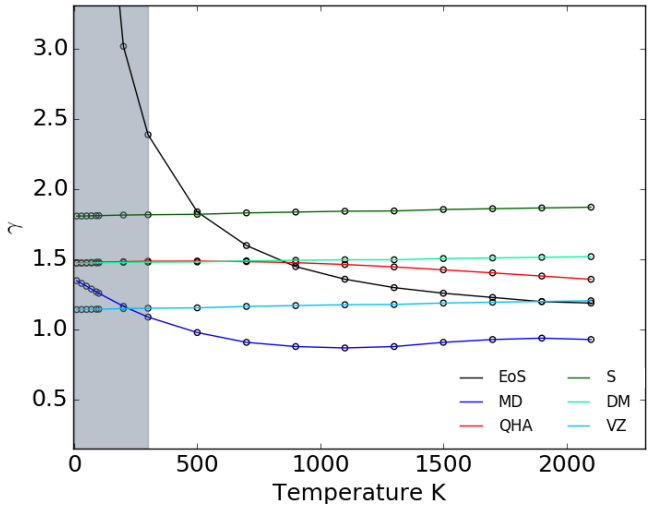

(a)

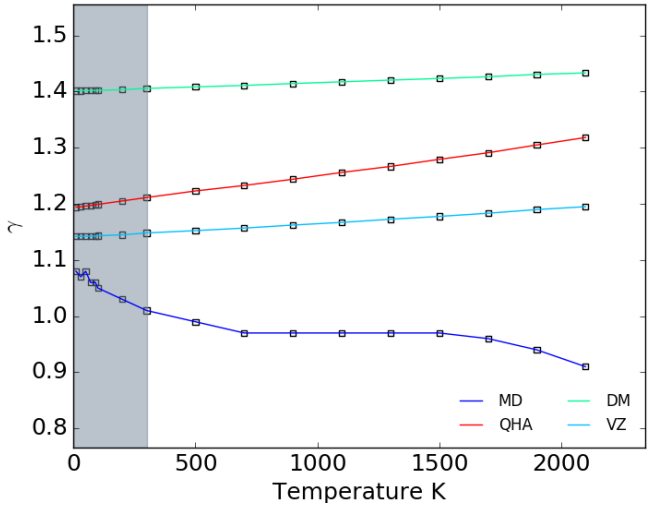

(b)

Figure 6.5: Comparison between the Gruneisen parameter its various models on Tantalum. The region below the Debye temperature is shown in gray. (a) Comparison for zero pressure calculations. (b) Comparison for calculations at 10 GPa. Note: MD = The true Gruneisen Parameter; QHA = Vibrational definition; EoS = Mie-Gruneisen definition; Sl = Slater definition; DM = Dugdale-MacDonald definition; and VZ = Vashchenko-Zubarev definition.

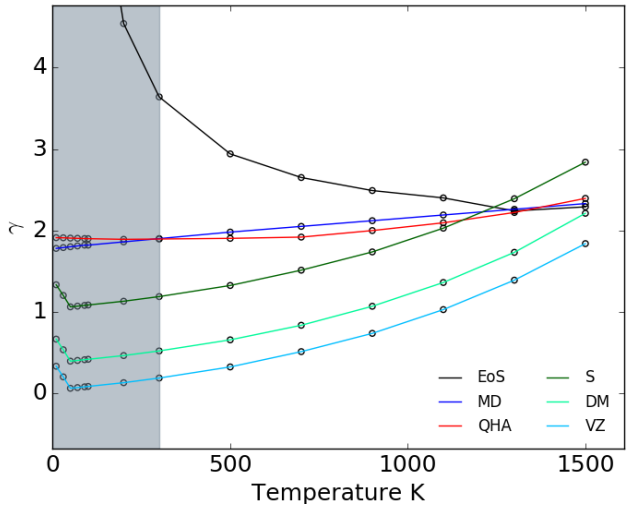

(a)

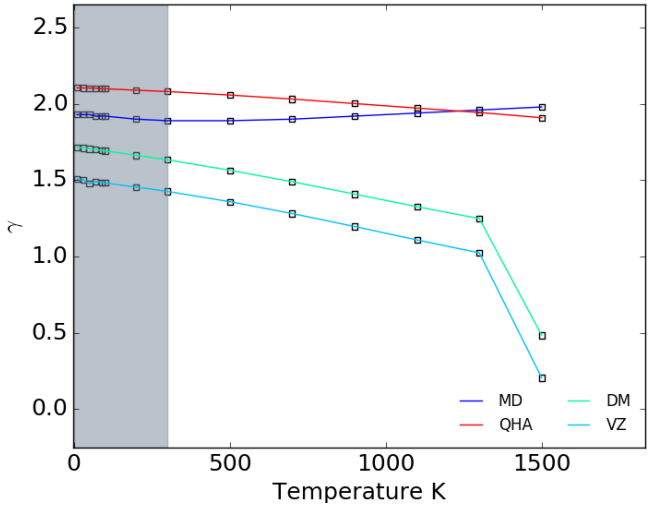

(b)

Figure 6.6: Comparison between the Gruneisen parameter its various models on Copper. The region below the Debye temperature is shown in gray. (a) Comparison for zero pressure calculations. (b) Comparison for calculations at 10 GPa. Note: MD = The true Gruneisen Parameter; QHA = Vibrational definition; EoS = Mie-Gruneisen definition; Sl = Slater definition; DM = Dugdale-MacDonald definition; and VZ = Vashchenko-Zubarev definition.

6.1 Future Work

Development of wider regime equations of state to describe the thermodynamic properties of solids should be a long term goal of our academic community. More immediate work can be done to correct the current models. The use of the density of states as a function of temperature to correct γ in the quasi-harmonic approximations is at hand. This new method proposes summing over a temperature dependent equation for the density of states rather that the current summation of modes.

Another way to help capture full anharmonic effects would be to expand the terms in the taylor expansion of energy. However, there are many terms to consider which will be difficult to implement. The inclusion of adjusting parameters from non-experimentalist sources such as DFT maybe a more feasible approach.

References

[1] V. Bushman, G.I. Kanel, A.L. Ni, V.E. Forvot, "Intense Dynamic Loading of Condensed Matter" Taylor and Francis, London, 1993.

[2] *Thermal Expansion, Metallic Elements and Alloys, Vol. 12 of Thermophysical Properties of Matter*, edited by Y. S. Touloukian, R. K. Kirby, R. E. Taylor, and P. D. Desai (Pleanum, New York-Washington, 1975).

[3] S.A. Miller, *et al.*, "Capturing Anharmonicity in a Lattice Thermal Conductivity Model for High-Throughput Predictions" *Chem. of Mater.*, 2017, No. 6, pp. 2494-2501.

[4] O.L. Anderson, "The Grulseren ratio for the last 30 years" *Geophys. J. Int.*, 2000, No. 143, pp. 279-293, and references therein.

[5] R. Ravelo, T.C. Germann, O. Gerrero, Q. An, and B.L. Holian, "Shock-induced plasticity in tantalum single crystals: Interatomic potentials and large-scale molecular-dynamics simulations," *Physics Review B*, 2013, No. 88, pp. 134101.

[6] Y. Mishin, *et al.*, "Structural stability and lattice defects in copper: Ab initio, tight-binding, and embedded-atom calculations," *Physics Review B*, 2001, No. 63, pp. 224106.

[7] A. Dewaele, P. Loubeyre, and M. Mezouar, *Phys. Rev.*, 2004, No. 70, pp. 094112.

[8] H. Cynn, and C. S. Yoo, *Phys. Rev.*, 1999, No. 59, pp. 0526.

[9] P. M. Bell, J. Xu, and H. K. Mao, "Shock Waves in Condensed Matter," Plenum Press, New York/London, 1985.

[10] J. Xu, H. K. Mao, and P. M. Bell, *High Temp.-High Press.*, 1984, No. 16, pp. 125.

[11] J.S. Dugdale, D.K.C. MacDonald, *Phys. Rev.*, 89, pp. 832, 1953.

[12] V.Ya. Vashchenko, V.N. Zubarev, *Sov. Phys. Solid State*, 5, pp. 653, 1963.

[13] J.C. Slater, "Introduction to Chemical Physics," MacGraw-Hill, New York, 1939.

[14] O.L. Anderson, "Simple solid-state equations for materials of terrestrial planet interiors" *The Physics of Plants* , S. K. Roundcorn ed., J. Wiley, London, No. 29, pp. 27-60, 1988.

[15] F. Quareni, and F. Mulargia, "The validity of the common approximate expressions for the Gruneisen parameter." *Geophys. J.*, 1988, No. 93, pp. 505-519.

[16] F. D Stacey, "Properties of a Harmonic lattice," *Phys. Earth Planet Interiors*, No. 15 pp. 341-348.

[17] S. A. Miller, *et al.*, "Capturing Anharmonicity in a Lattice Thermal Conductivity Model for High-Throughput Predictions," *Chem. of Mater.*, 2017, No. 8 pp. 2494-2501.

[18] J. Yan, *et al.*, "Material descriptors for predicting thermoelectric performance," *Energy Environ. Sci.*, 2015, 8, 983?994. 534.

[19] V. N. Zharkov, V.A. Kalinin, "Equations of State for Solids at High Pressure and Temperature." Consultants Bureau, New York, 1971.

[20] L. Vovadlo, J. P. Poirer, and G. D. Price, *Amercian Mineralogist*, 2000, Vol 85.

[21] J. P. Poirier, *Introduction to the physics of the Earth's Interior*, 1991.

[22] O.L. Anderson, "A universal thermal equation of state" *J. Geodynamics*, No. 1, pp. 185-214, 1984.

[23] R. E. Cohen, and O. Grulseren, "Thermal Equations of State of Tantalum" *Phys. Rev. B*, 2001, No. 63, pp. 224101.

[24] A. J. Falzone, and F. D. Stacey, "Second order elasticity theory: explanation for the high Poisson's ratio of the inner core, " *Phys. Earth Planet. Inter.*, 1980, No. 21, pp. 371-377.

[25] M.P. Allen, *Introduction to Molecular Dynamics Simulations* NIC Series, 2004, No. 23, pp. 1-28.

[26] D. L. Anderson, "A seismic equation of states, II. Shear properties and Thermodynamics of the lower mantle," *Phys. Earth Planet Interiors*, 1987, No. 45 pp. 307-323.

[27] D. L Anderson, "Thermally induced phase changes, lateral heterogeneity of the mantle, continental roots and deep slab anomalies," *J. Geophys, Res.*, 1987, No. 92 pp. 13968-13980.

[28] D. L Anderson, "Temperature and pressure derivatives of elastic constants, with application to the mantle," *J. Geophys. Res.*, 1988, No. 93 pp. 4668-4700.

[29] W. Peter, "An Introduction to Ergodic Theory" Springer, 1982.

[30] M. Allen, and D. Tildesley, "Computer Simulation of Liquids," Clarendon Press, New York, 1989.

[31] S. Nosè, "Molecular Physics," 1984, No. 52 pp. 255.

[32] T. H. K. Barron, "Gruneisen parameters for the equation of state of solids." *Annals of Physics*, 1, pp. 77-90, 1957.

[33] L. Burakovsky, D.L. Preston, Y. Wang, "Cold Shear Modulus and Gruneisen Parameter at all Densities" *Sol. St. Com.*, 2004, No.132, pp. 151-156.

[34] R. H. Carr, "Use of mutual inductance techniques to measure thermal expansion at low temperatures," *Retrospective Theses and Dissertations*, Iowa State University, 1963.

[35] G. R. Clusener, "Economy Considerations for Pushrod-Type Dilatometers," Thermal Expansion American Institute of Physics, New York, 1972.

[36] M.S. Daw, and M.I. Baskes, *Physics Review B*, 1984, No. 29, pp. 6443.

[37] F.R. de Boer, R. Boom, W.C.M. Mattens, A.R. Miedema, and A.K. Niessen, *Cohesion in Metals: Transition Metal Alloys*, Elsevier Scientific, New York, 1988.

[38] D. B. Fraser, and A. C. Hollis-Hallett, "The Coefficinet of Linear Expansion and Gruneisen Gamma of Cu, Ag, Au, Fe, Ni, and Al from 4 to 300 K," *Proc. Int. Conf. Low Temperature Phys.*, 1961, No. 7 pp. 689-692.

[39] G. Grimvall, "Thermodynamic Properties of Materials," Elsevier, Amsterdam, 1999. Enlarged and revised edition.

[40] E. Gruneisen, "Theorie des festen zustandes einatomiger element," *Annals Physik*, 12, pp. 257-306, 1912.

[41] F.A. Jenkins, and H.W. White, "Fundamentals of Optics," McGraw-Hill, New York, 1957.

[42] C. Kittel, "Introduction to Solid State Physics," Wiley-Interscience, New York, 1986.

[43] L. Knopoff, and J. N. Shapiro, "Comments on the inter-relationships between Gruneisen's parameter and shock and isothermal equations of state, " *J. Geophys. Res.,*, 1969, No. 74, pp. 1439-1450.

[44] J.F. Kos, and J.L.G. Lamarche, "Thermal Expansion of the Noble Metals below 15 K," *Can. J. Phys.*, 1996, No. 47 pp. 2509-2518.

[45] *Refractory Metals and Refractory Metal Alloys, In: Springer Handbook of Materials Data*, written by W. Knabl et. al. Edited by H. Warlimont, and W. Martienssen (Springer, Cham, 2018).

[46] Yu. A. Lisovskii, "Analysis of Thermal Expansion of Transition Metals in the Quasi-harmonic Approximation," *Fiz. Tverd. Tela.*, 1972, No. 14(8) pp. 2329-2333; English Translation: Sov. Phys. -Solid State, 1973, No. 14(8) pp. 2015-2018.

[47] H. Liu, H. Song, Q. Zhang, G. Zhang, Y. Zhao, "Validation for equations of state in wide regime: Copper as prototype." *Matter and Radiation at Extremes*, 1, pp. 123-131, 2016.

[48] Y. Mishin, D. Farkas, M. J. Mehl, and D. A. Papaconstantopoulos, *Multiscale Modelling of Materials*, edited by V. V. Bulatov, T. Diaz de la Rubia, R. Phillips, E. Kaxiras, and N. Ghoniem, MRS Symposia Proceedings No. 535 (Materials Research Society, Warrendale, Pennsylvania, 1999)

[49] P. D. Pathak and N.G. Vasavada, "Thermal Expansion and he Law of Corresponding States," *J. Phys. C (Solid State Phys.)*, 1970, No. 3(2) pp. L44-L48.

[50] G. Simons, and H. Wang, "Single Crystal Elastic Constants and Calculated Aggregate Properties," MIT Press, Cambridge, MA, 1977.

[51] "Metal Reference Book," edited vy C.J. Smith, Butter-worth, London, 1986.

[52] W.L. Stewart, J.M. Roberts, N.G. Alexandropolous, and K. Salama, *J. Appl. Phys.*, 1977, No. 48, pp. 75.

Vita

Celia Garcia Amparan was born as the second child of Antonio Garcia Rascon and Celia Amparan Velador de Garcia. She graduated from Mission Early College High School in El Paso, TX. After obtaining her Associates of Art in 2010 at the age of 17, she entered The University of Texas at El Paso where she completed her bachelors degree in Applied Physics. She later entered the Graduate School to pursue a Masters degree in Metallurgy and Materials Engineering.

Permanent email address: cgarcia38gn3@gmail.com